ACSNANO

www.acsnano.org

ARTICLE

Ionizable Lipid Nanoparticles for Therapeutic Base Editing of Congenital Brain Disease

Rohan Palanki,● Sourav K. Bose,● Apeksha Dave, Brandon M. White, Cara Berkowitz, Valerie Luks, Fazeela Yaqoob, Emily Han, Kelsey L. Swingle, Pallavi Menon, Emily Hodgson, Arijit Biswas, Margaret M. Billingsley, Li Li, Fan Yiping, Marco Carpenter, Alexandra Trokhan, Julie Yeo, Nuryanti Johana, Tan Yi Wan, Mohamad-Gabriel Alameh, Frederick Chris Bennett, Phillip B. Storm, Rajan Jain, Jerry Chan, Drew Weissman, Michael J. Mitchell,* and William H. Peranteau*

Cite This: https://doi.org/10.1021/acsnano.3c02268 Read Online

ACCESS | Metrics & More | Article Recommendations | Supporting Information

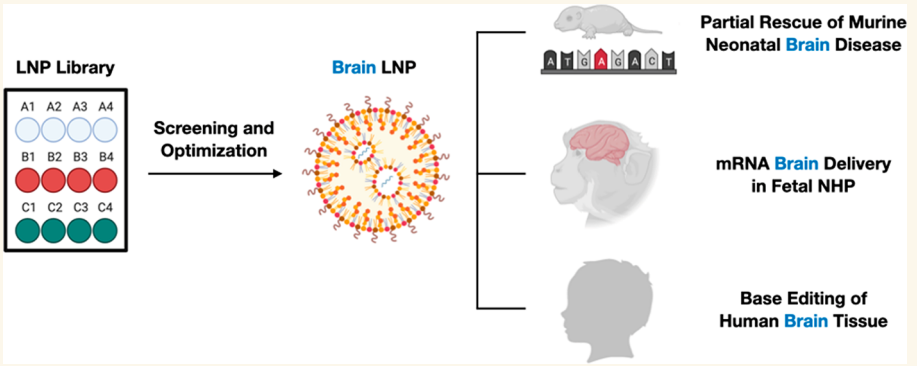

ABSTRACT: **Delivery of mRNA-based therapeutics to the perinatal brain holds great potential in treating congenital brain diseases. However, nonviral delivery platforms that facilitate nucleic acid delivery in this environment have yet to be rigorously studied. Here, we screen a diverse library of ionizable lipid nanoparticles (LNPs) via intracerebroventricular (ICV) injection in both fetal and neonatal mice and identify an LNP formulation with greater functional mRNA delivery in the perinatal brain than an FDA-approved industry standard LNP. Following *in vitro* optimization of the top-performing LNP (C3 LNP) for codelivery of an adenine base editing platform, we improve the biochemical phenotype of a lysosomal storage disease in the neonatal mouse brain, exhibit proof-of-principle mRNA brain transfection *in vivo* in a fetal nonhuman primate model, and demonstrate the translational potential of C3 LNPs *ex vivo* in human patient-derived brain tissues. These LNPs may provide a clinically translatable platform for *in utero* and postnatal mRNA therapies including gene editing in the brain.**

KEYWORDS: *ionizable lipid nanoparticles, congenital brain disease, mRNA delivery, gene editing, fetal gene therapy*

INTRODUCTION

Approximately 7,000−10,000 diseases result from mutations in single genes, of which 17% have a neurologic component including developmental delay, motor and cognitive dysfunction, and progressive neuronal degeneration.[1−4] Although some genetic diseases, including inborn errors of metabolism, that affect the CNS can be treated with enzyme replacement therapies, few curative therapies exist and current clinical management often focuses on symptom reduction.[1,2] The pathology of many genetic CNS diseases begins before birth and is difficult to reverse after onset resulting in significant morbidity by the time of or shortly after birth.[3] Progress in prenatal care and DNA sequencing technology now allows for the prenatal diagnosis of many genetic diseases, including the identification of disease-causing mutations, highlighting the potential to treat disease before birth and the onset of irreversible pathology.[4]

Advances in mRNA-based gene editing tools, including CRISPR-Cas9 and base editing platforms, provide an

Received: March 10, 2023
Accepted: July 13, 2023

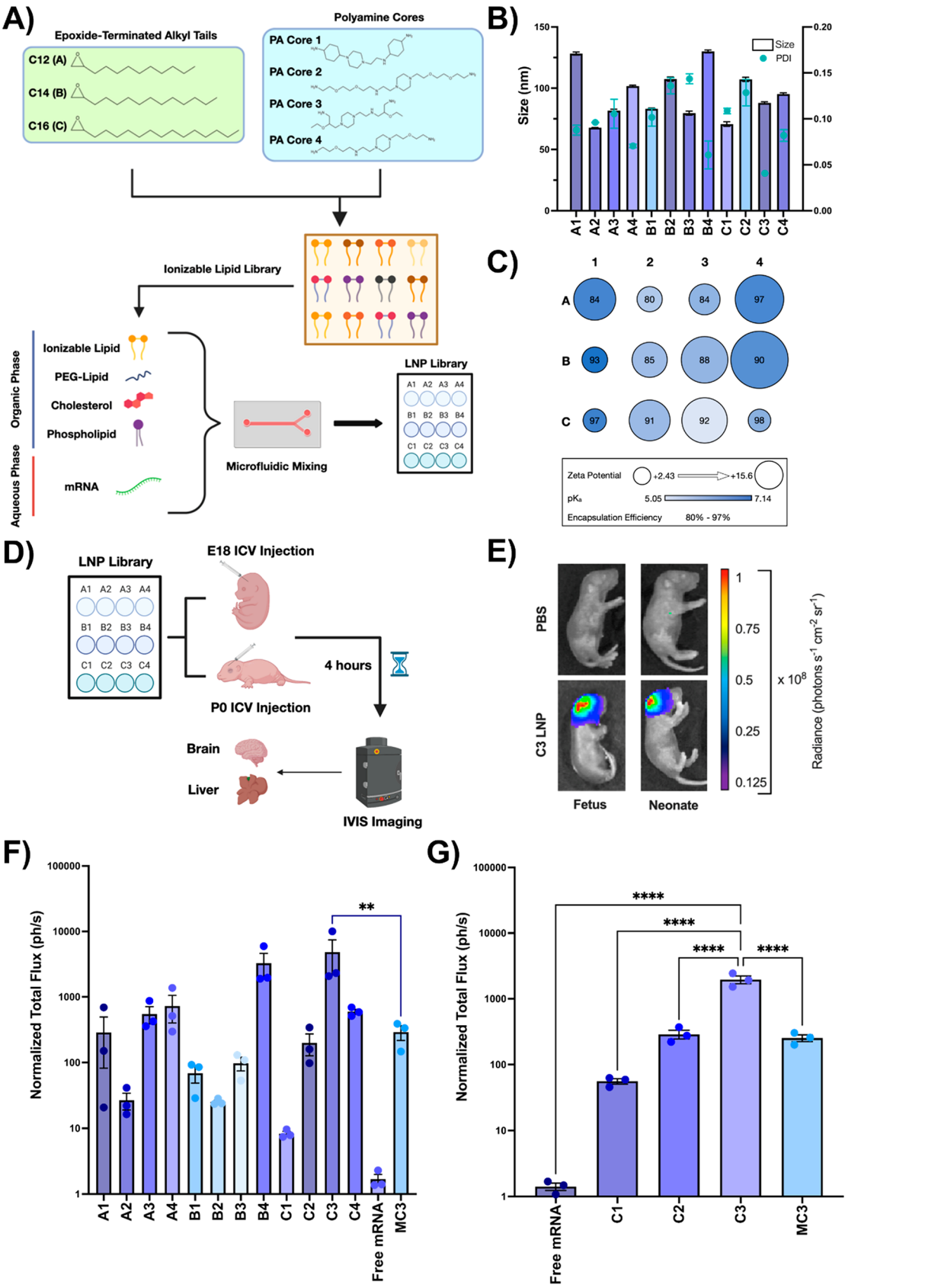

Figure 1. | Design and evaluation of LNP library for perinatal brain mRNA delivery. (A) Chemical structures of epoxide-terminated alkyl tails (green box) and polyamine cores (blue box) combined to generate an ionizable lipid library. Formulation of LNPs via microfluidic mixing with an ethanol phase containing ionizable lipid, PEG-lipid, cholesterol, and DOPE and an aqueous phase containing *luciferase* mRNA is also visualized. LNPs were named based on the alkyl tail length (A−C) and polyamine core (1−4) of the ionizable lipid incorporated into the formulation. (B) Size and PDI of each LNP formulation in the LNP library. (C) Zeta potential (radius of circle), pK_a

https://doi.org/10.1021/acsnano.3c02268
ACS Nano XXXX, XXX, XXX−XXX

Figure 1. continued

(gradient color), and encapsulation efficiency (centered number) for each LNP formulation. (D) Scheme demonstrating LNP screening in E18 BALB/c fetuses or P0 BALB/c neonates via ICV injection. (E) IVIS imaging showing *luciferase* expression in a representative C3 LNP-treated fetus (left) and neonate (right) relative to PBS-treated controls. (F) Quantification of luciferase signal from fetal brains treated with each LNP. (G) Quantification of luciferase signal from the neonatal brains treated with a subset of LNPs. All luminescence readings are represented as normalized total flux. **$p < 0.01$, ****$p < 0.0001$ by one-way analysis of variance (ANOVA) with posthoc Dunnett's test compared to MC3 (fetus) and C3 (neonate). Outliers were detected using Grubbs' test and removed from analysis; minimum $n = 3$ per treatment group; error bars represent SEM.

opportunity for "one-and-done" treatments for monogenic diseases.[5,6] *In utero* gene editing takes advantage of normal fetal ontogeny to deliver therapies in a potentially more efficient manner, mitigating genetic disease before pathologic insult. Specifically, small fetal size maximizes dose of a therapy per recipient weight, fetal stem/progenitor cells are more accessible and abundant supporting the persistence of the therapeutic edit, and a tolerant fetal immune system minimizes an immune barrier to gene editing tools.[4] Previously, we demonstrated the therapeutic potential of *in utero* gene editing in mouse models of human diseases, rescuing the lethal phenotype of hereditary tyrosinemia type 1, improving the pulmonary phenotype of surfactant protein C deficiency, and ameliorating metabolic, musculoskeletal, and cardiac disease in mucopolysaccharidosis type I (MPS-IH, Hurler syndrome).[7−9] These proof-of-concept studies demonstrated the ability to efficiently target the fetal liver and heart following intravascular delivery of a viral vector and pulmonary epithelial cells following intra-amniotic delivery of a viral vector. Although encouraging, CNS targeting via these approaches was not efficient, highlighting the need to evaluate alternative delivery approaches to treat CNS diseases.

Although viral vectors have potential to deliver gene editing technology to the CNS, viral delivery platforms can be limited by pre-existing viral immunity, transgene size constraints, undesired vector integration, and adverse events related to the viral vector.[10−12] Ionizable lipid nanoparticles (LNPs) are a promising nonviral delivery platform for mRNA nanomedicines[13,14] that have been used to deliver siRNA and CRISPR-based gene editing therapies to the liver in postnatal mouse, nonhuman primate, and clinical studies with encouraging results.[15−18] A distinct advantage of using LNPs is their modularity, but this necessitates designing LNPs specifically for the target delivery location, intended cargo, and intended patient population, including the developmental stage of the patient. We previously identified LNPs for mRNA delivery to the fetal mouse liver following *in utero* intravascular injection.[19] These studies demonstrate the potential of LNPs as a delivery platform for nucleic-acid-based therapies, including gene editing technologies, especially for diseases amenable to liver targeting. However, the applicability of LNPs for genetic CNS diseases—as delivery vehicles for gene editing platforms in the perinatal brain—remains to be determined.

In the current study, we engineer LNPs for the delivery of mRNA base editing platforms to the perinatal brain. We first screen a diverse library of LNPs *in vivo* to identify LNPs that strongly transfect the fetal and neonatal mouse brain following intracerebroventricular (ICV) injection. After determining the cellular tropism of our top performing LNP in the perinatal mouse brain, we optimized the LNP formulation *in vitro* for three formulation parameters relevant to base editing applications. Optimized LNPs were then used to deliver adenine base editor (ABE) mRNA and synthetic guide RNA (sgRNA) by ICV injection in the neonatal mouse model of MPS-IH to correct the *Idua* G → A (W392X) disease-causing mutation. We demonstrate successful LNP-mediated on-target base editing, improved biochemical parameters of the disease, and minimal immunologic response to the delivery vector. The same LNP formulation was then used to deliver mRNA to the brain in a fetal cynomolgus macaque following ICV injection. Finally, we demonstrate the translational potential of this delivery platform by confirming the stability of the optimized LNP in human cerebrospinal fluid (CSF), exhibiting LNP-mediated mRNA transfection in patient-derived neurons, and displaying LNP-mediated base editing of the human *IDUA* gene at the site of the common MPS-IH disease-causing mutation in human precision cut brain slices.

RESULTS

Synthesis and Characterization of an Ionizable LNP Library. A library of 12 LNPs was prepared as previously described.[20] First, ionizable lipids were synthesized using Michael addition chemistry, whereby alkyl tails (denoted by tail length: A = C12, B = C14, C = C16) were reacted with polyamine molecules (labeled numerically 1 through 4) to form polyamine-lipid cores. These ionizable lipids were combined with cholesterol, 1,2-dioleoyl-*sn*-glycero-3-phosphoethanolamine (DOPE), and lipid-anchored PEG at ratios determined by previous optimization studies in adult mice[21] and then mixed with firefly *luciferase* mRNA through a herringbone-style microfluidic device (Figure 1A).

The resultant library of LNPs was characterized by size, encapsulation efficiency, pK_a, and zeta potential (Table S1). Hydrodynamic diameter for all LNP formulations—measured via dynamic light scattering intensity—ranged from 67.8 to 128.3 nm with a maximum polydispersity value of 0.154 (Figure 1B), indicating small and relatively monodisperse LNPs (PDI < 0.3).[19] Encapsulation efficiencies were also high, ranging from 79.9% to 97.6% (Figure 1C). Next, LNPs were assessed for their pK_a, which reflects their ability to undergo endosomal escape and release nucleic acid cargo. All LNP formulations had a pK_a value between 5.05 and 7.14 (Figure 1C), which is within an acceptable range for *in vivo* nucleic acid delivery.[22] Finally, the zeta potential, a function of surface charge, was measured via a Zetasizer Nano.[23] In this library, LNP zeta potentials ranged from 15.6 to 2.43 mV (Figure 1C).

LNP-Mediated mRNA Delivery to the Perinatal Mouse Brain. After characterizing the LNP library, we evaluated it for mRNA delivery to the brain in fetal and neonatal BALB/c mice (Figure 1D). LNPs encapsulating *luciferase* mRNA at an mRNA dose of 1 mg/kg were injected ICV into the lateral ventricles of gestational day 18 (E18) BALB/c fetuses, a neuro-developmental stage akin to a midgestation human fetus and a time point where therapeutic intervention is technically feasible.[24] ICV injection was selected as the mode of introduction since it has been used

https://doi.org/10.1021/acsnano.3c02268
ACS Nano XXXX, XXX, XXX−XXX

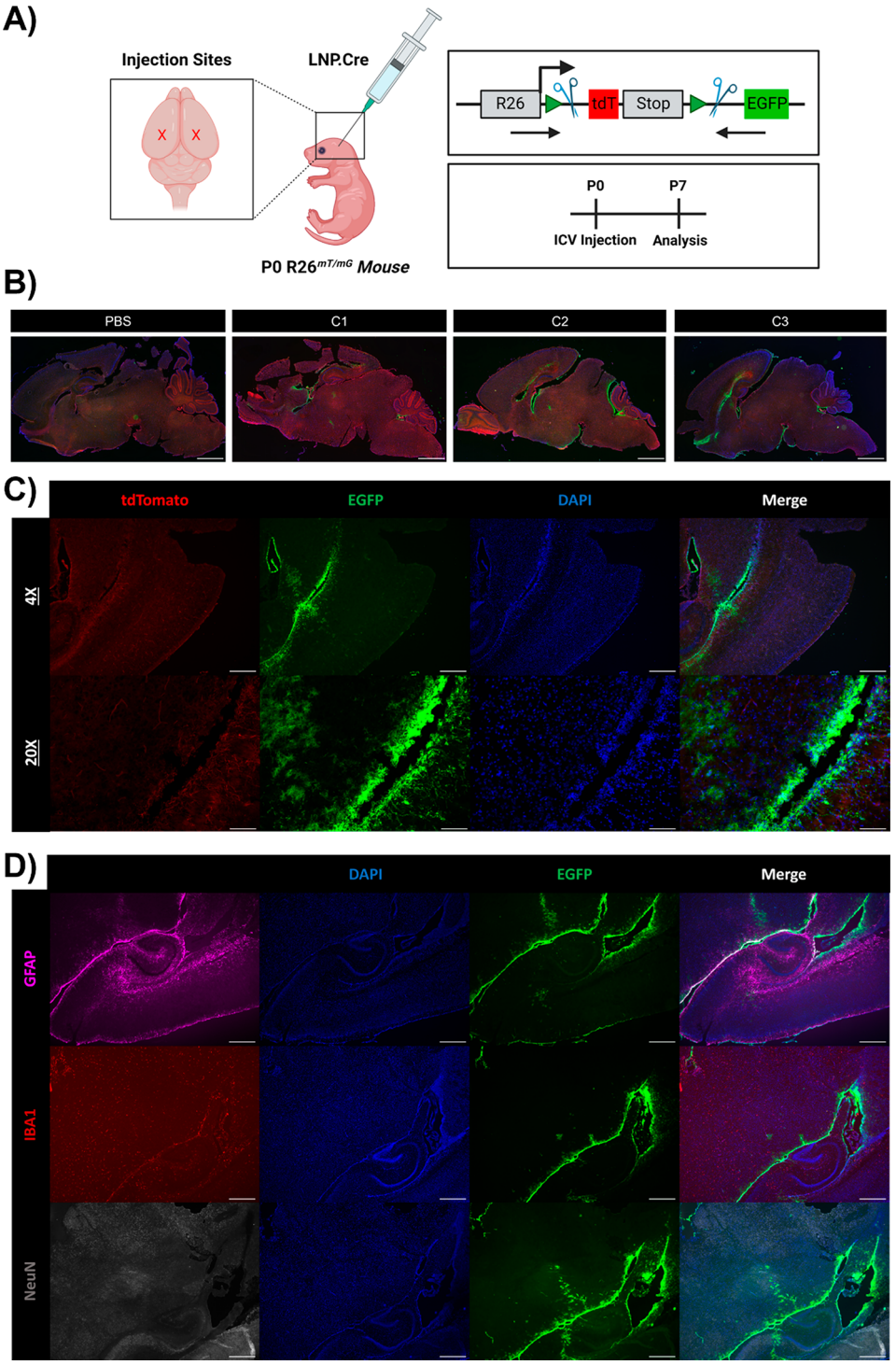

Figure 2. | Cellular tropism of C3 LNPs in the neonatal mouse brain. (A) Scheme demonstrating application of LNPs encapsulating *Cre* mRNA to P0 R26$^{mT/mG}$ neonates via bilateral ICV injection. Genome modulation in the R26$^{mT/mG}$ mouse model and experimental scheme are also visualized in the right panel. (B) Whole brain histology of neonatal brains 7 days after PBS, C1, C2, or C3 LNP ICV injection, displaying unedited (tdTomato+) and edited (GFP+) regions, imaged at 1×. (C) Histology focused on the brain ventricular lining 7 days after C3 LNP ICV injection, imaged at 4× and 20×. (D) Histology focused on the brain ventricular lining with intracellular staining to capture successful C3 LNP-mediated delivery (GFP+) to astrocytes (GFAP+), microglia (IBA1+), and neurons (NeuN+). Scale bars: 1 mm (1×), 200 μm (4×), and 50 μm (20×).

clinically to safely and effectively deliver therapeutic agents for a broad range of neurological diseases.[25] Fetuses were assessed 4 h after ICV injection for luciferase expression using an *in vivo* imaging system (IVIS). This time point was selected based on previous studies[19,26] and *in vitro* verification of LNP-mediated luciferase expression by 4 h (Figure S1). For each injected dam, phosphate-buffered saline (PBS) injected fetuses served as negative controls. Naked *luciferase* mRNA was included as a treatment group to demonstrate baseline nucleic acid uptake in the brain without an LNP carrier. Finally, DLin-MC3-DMA

https://doi.org/10.1021/acsnano.3c02268
ACS Nano XXXX, XXX, XXX−XXX

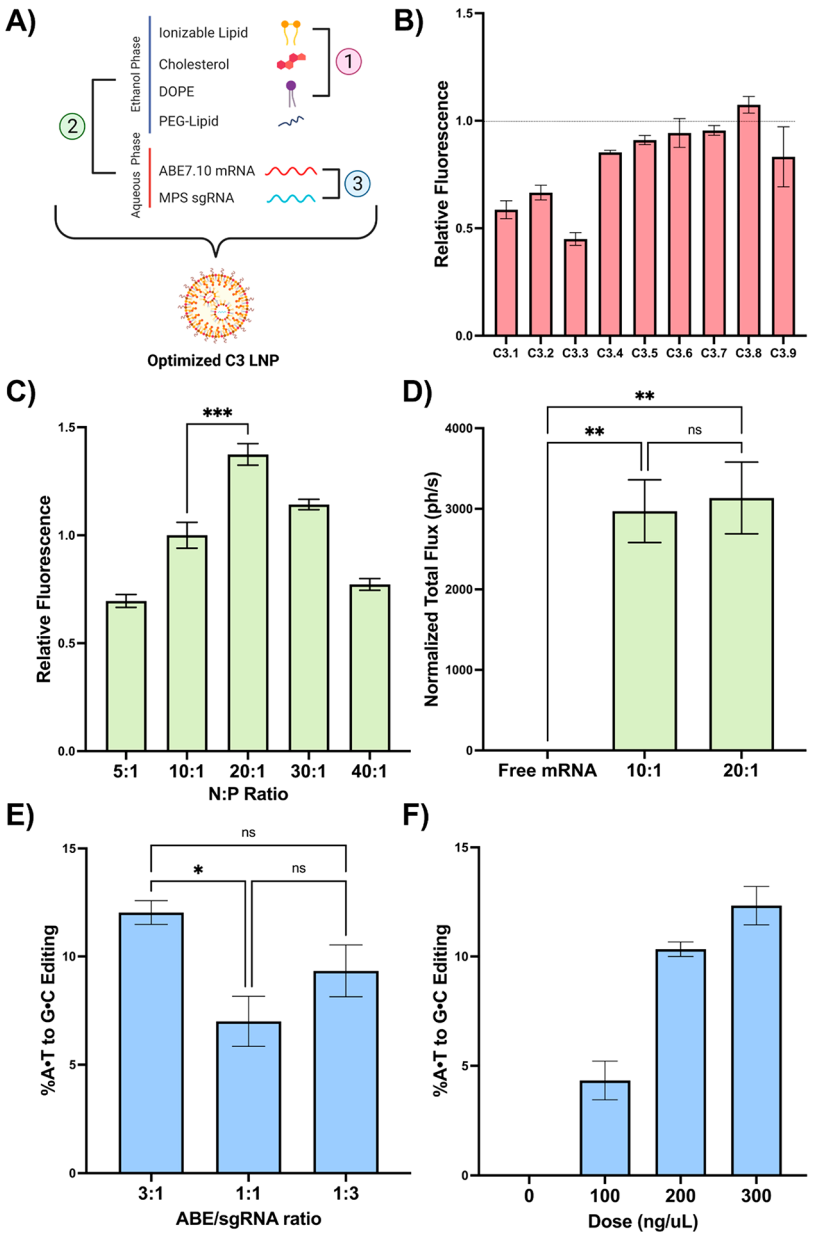

Figure 3. | *In vitro* optimization of C3 LNPs for codelivery of base editing platforms. (A) Scheme demonstrating the three LNP formulation parameters evaluated: (1) excipient molar ratios, (2) N:P ratio, and (3) ABE to sgRNA mass ratio. (B) Normalized mean fluorescence intensity (MFI) in Neuro-2a cells after treatment with the C3 LNP DOE library relative to the original C3 LNP formulation (dotted line). (C) Normalized MFI in Neuro-2a cells after treatment with C3 LNPs formulated at a range of N:P ratios. (D) Quantification of luminescence signal (normalized total flux) from brains of neonates treated with C3 LNPs prepared at the top-performing N:P ratios *in vitro*. (E) Sequencing results at the expected site of base editing following C3 LNP-mediated base editing in primary MPS-I murine fibroblasts at three ABE/sgRNA mass ratios. (F) Sequencing results in primary MPS-I murine neurons treated with C3.MPS LNPs at a range of doses. *$p < 0.05$, **$p < 0.01$, ***$p < 0.001$ by one-way ANOVA with posthoc Dunnett's test compared positive controls described in the text. Outliers were detected using Grubbs' test and removed from analysis; minimum $n = 3$ replicates per treatment group; error bars represent SEM.

ionizable lipid—an FDA approved industry standard[18]—was used to encapsulate *luciferase* mRNA as a positive control.

IVIS imaging of both the whole fetus (Figure 1E) and individually dissected fetal brains (Figure 1F) demonstrated a range of mRNA delivery and luciferase expression in the brain with all LNPs in the library. All LNP formulations yielded greater mRNA delivery than injection of naked mRNA, confirming that LNP encapsulation protects mRNA cargo from systemic degradation and facilitates intracellular delivery (Figure 1F). Each ionizable lipid produced LNPs with variable performance, demonstrating the crucial role of this component in mRNA delivery (Figure 1F). Interestingly, we observed trends for *in vivo* transfection efficacy in the fetal brain with decreasing pK_a, increasing size, and increasing zeta potential (Figure S2). The top-performing LNP (C3 LNP) resulted in 17-fold greater mRNA expression in the fetal brain than the industry standard ($p < 0.05$). Of note, IVIS imaging of individually dissected fetal livers demonstrated minimal luciferase expression after treatment with any of the LNPs in this library (Figure S3). Finally, we assessed the *in vivo* biodistribution of C3 LNPs administered ICV to E18 Balb/c fetuses. We observed strong luciferase expression in the fetal

https://doi.org/10.1021/acsnano.3c02268
ACS Nano XXXX, XXX, XXX−XXX

brain but no significant expression in the heart, lung, intestine, liver, spleen, or kidney relative to a PBS-injected control (Figure S4).

In this *in vivo* screen, long-term survival postinjection was not assessed. However, fetal mouse ICV injection has previously been associated with intrauterine mortality due to the technical challenge of this procedure in small animals.[27] In contrast, postnatal day 0 (P0) mouse ICV injections are technically easier, associated with good long-term survival, and still approximate the CNS development of a mid-to-late gestation human fetus. Therefore, additional studies were performed to determine whether the results of LNP-mediated mRNA delivery to the fetal mouse brain were maintained following ICV administration to neonatal mice. LNPs identified as high- (C3), mid- (C2), and low-performing (C1) in the fetal ICV screening studies, the industry standard LNP (MC3), or free *luciferase* mRNA were injected ICV at an mRNA dose of 1 mg/kg in P0 BALB/c neonates. Survival at 4 h after neonatal ICV injection, the terminal analysis time point, was 100% in Balb/c neonates. IVIS imaging of neonatal brains confirmed the performance trends observed in the fetal brain (Figures 1F and 1G), with C3 LNPs facilitating 8-fold greater mRNA expression in the neonatal brain than the industry standard LNP ($p < 0.0001$). These results, in combination with improved experimental feasibility, supported the use of neonatal mouse models in subsequent studies.

C3 LNPs Facilitate Gene Modulation in Periventricular Cells of the Murine Brain. To gain insight into the cellular tropism of LNP-mediated mRNA delivery in the neonatal brain, we studied the brain biodistribution of high- (C3), mid- (C2), and low-performing (C1) LNPs containing *Cre* recombinase mRNA (1 mg/kg) after ICV administration to P0 $R26^{mT/mG}$ mice. $R26^{mT/mG}$ mice contain a membrane-targeted tdTomato (mT) cassette flanked by *loxP* sites and constitutively express red fluorescence in all cells (Figure 2A). Upon expression of translated Cre protein, the mT cassette and transcriptional stop cassette are deleted, resulting in the expression of a downstream mG-enhanced green fluorescent protein (mG-EGFP) cassette. Thus, successful LNP-mediated delivery of *Cre* mRNA leads to expression of green fluorescence in the transfected cell.

Survival after neonatal ICV injection was 100% in $R26^{mT/mG}$ neonates. One week after injection, harvested neonatal brains were analyzed for gene modulation via tissue histology. Although we observed similarities in whole brain distribution across LNPs, the magnitude of GFP expression and was proportional to LNP performance in our initial screening studies (C3 > C2 > C1) (Figure 2B). None of the LNPs demonstrated significant diffusion deep into the brain parenchyma beyond the periventricular space. C3 LNP-treated neonates had strong GFP expression in the periventricular areas and adjacent cortical structures (Figures 2B and 2C). Flow cytometry (Figure S5) and cell-specific brain histology (Figure 2D) confirmed GFP expression in microglia lining the ventricles, vicinal astrocytes, and neurons with limited penetration to internal brain structures. Despite low whole brain gene modulation and delivery to specific brain cells or internal brain structures, efficient targeting of periventricular cells is a potential target to produce therapeutic proteins for secretion into CSF circulation and utilize a paracrine effect for treatment of disease.

***In Vitro* Optimization and Validation of C3 LNPs for Codelivery of Base Editing Technology.** The molar ratios at which the components of LNPs are combined can be optimized for specific applications to better encapsulate nucleic acid cargo, enhance uptake by target cells, or alter biodistribution and protein corona formation.[28] In our initial library screen, LNPs were formulated with standard parameters known to facilitate mRNA delivery. However, the optimal parameters to produce C3 LNPs specifically for base editing applications in the brain were unknown. Thus, we used a multistage optimization protocol to determine the effects of excipient molar ratio, N:P ratio, and ratio of codelivered mRNA on C3 LNP delivery performance in neural-origin cell lines (Figure 3A).

While the ionizable lipid—in this case C3—is a major determinant of intracellular delivery by both directly complexing with mRNA and facilitating endosomal escape, the remaining excipients also play critical roles: cholesterol provides stability and enables membrane fusion, DOPE supplies structural support, and PEG reduces aggregation and nonspecific endocytosis.[29] In prior work, we demonstrated that modulating excipient molar ratios improves *in vitro* delivery to fetal lung cells and corresponds to enhanced *in vivo* performance following intra-amniotic LNP injection.[28] Here, we used an orthogonal design of experiments (DOE) methodology to investigate a design space of 27 LNP formulations, generated using three molar ratios each of C3 ionizable lipid, cholesterol, and DOPE with a fixed PEG-lipid ratio (Figure S6). A representative library of 9 LNPs encapsulating GFP mRNA (C3.1—C3.9) was screened against the original C3 LNP (C3.0) for delivery and cytotoxicity in Neuro-2a cells—immortalized mouse neuroblasts isolated from brain tissue. Although none of these formulations significantly enhanced mRNA delivery compared to the original C3 LNP formulation (Figure 3B), we did identify relationships between the molar ratio of each excipient and mRNA delivery (Figure S7). Of note, these trends are distinct from those observed in our prior studies that utilized different ionizable lipids,[28,30] demonstrating the importance of exploring these parameters in an application-specific manner. For all future studies, C3 LNPs were formulated at a molar ratio of 35:16:46.5:2.5 of C3 ionizable lipid, DOPE, cholesterol, and PEG, respectively.

The N:P ratio is the quantitative relationship between nitrogen on the ionizable lipid to phosphate groups on mRNA. Previous studies have demonstrated that the N:P ratio impacts both nucleic acid delivery and toxicity, with higher ratios leading to diminishing returns in cellular transfection due to increased cell death.[31] The ideal N:P ratio is known to be distinct for each ionizable lipid.[18] As such, C3 LNPs were formulated at a range of N:P ratios to encapsulate *GFP* mRNA and were screened for delivery and cytotoxicity in Neuro-2a cells. In comparison to the original N:P ratio of 10:1, LNPs formulated at an N:P ratio of 20:1 had a significant improvement in mRNA delivery (Figure 3C, $p < 0.001$) albeit with enhanced toxicity (Figure S8B). To explore if this improvement was maintained *in vivo*, C3 LNPs were formulated with *luciferase* mRNA at both 10:1 and 20:1 N:P ratios and injected ICV in P0 BALB/c mice. IVIS imaging revealed that while both LNP formulations had similar performance in the neonatal mouse brain to the initial screening study, there was no significant difference between the LNPs formulated at different N/P ratios (Figure 3D). Given the increased *in vitro* toxicity seen with the 20:1 N:P ratio and to minimize reactive excess ionizable lipid in solution,

https://doi.org/10.1021/acsnano.3c02268
ACS Nano XXXX, XXX, XXX−XXX

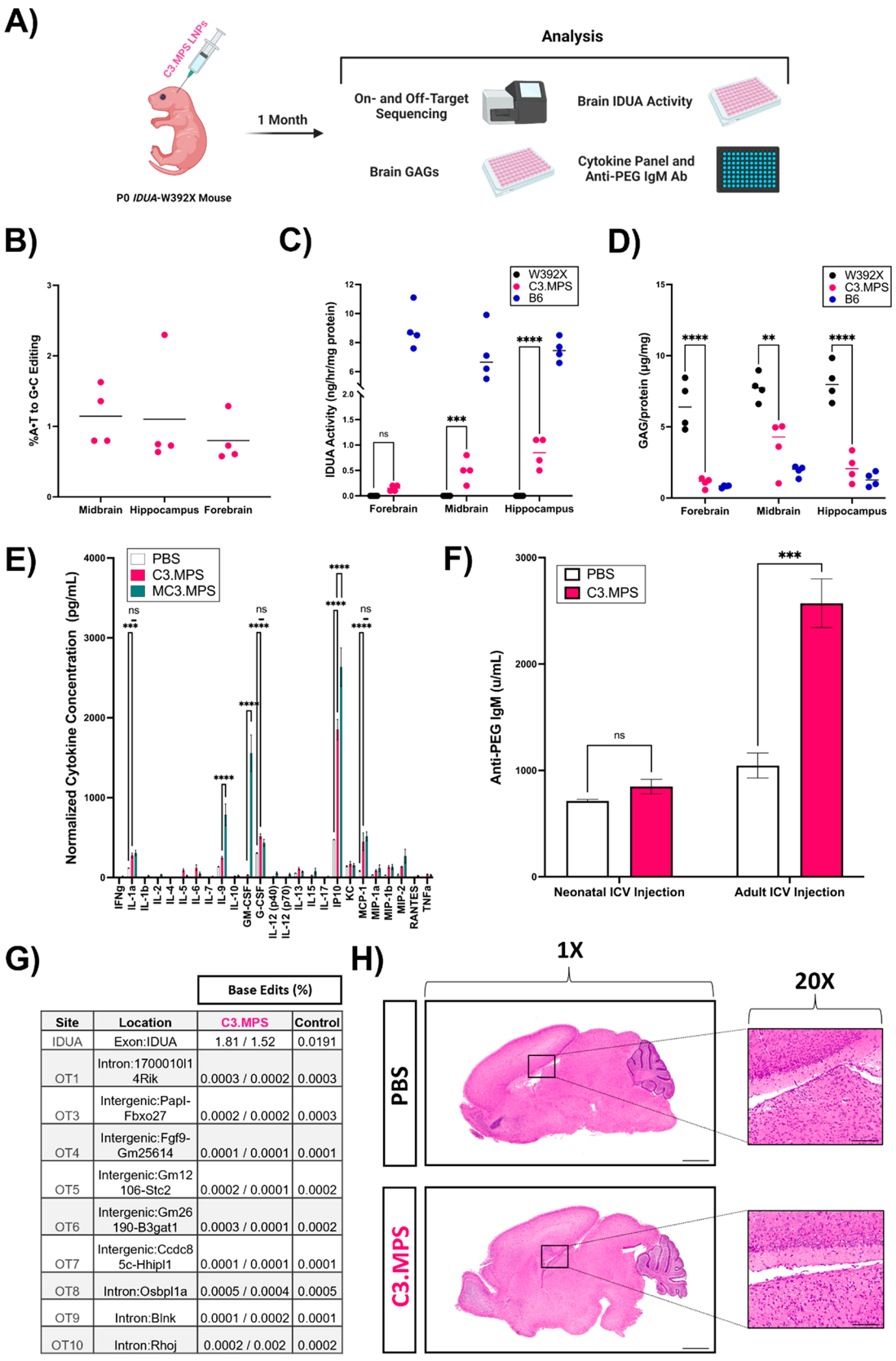

		Base Edits (%)	
Site	Location	C3.MPS	Control
IDUA	Exon:IDUA	1.81 / 1.52	0.0191
OT1	Intron:1700010I14Rik	0.0003 / 0.0002	0.0003
OT3	Intergenic:Papl-Fbxo27	0.0002 / 0.0002	0.0003
OT4	Intergenic:Fgf9-Gm25614	0.0001 / 0.0001	0.0001
OT5	Intergenic:Gm12106-Stc2	0.0002 / 0.0001	0.0002
OT6	Intergenic:Gm26190-B3gat1	0.0003 / 0.0001	0.0002
OT7	Intergenic:Ccdc85c-Hhipl1	0.0001 / 0.0001	0.0001
OT8	Intron:Osbpl1a	0.0005 / 0.0004	0.0005
OT9	Intron:Blnk	0.0001 / 0.0002	0.0001
OT10	Intron:Rhoj	0.0002 / 0.002	0.0002

Figure 4. |Efficacy and safety of C3.MPS LNPs in *Idua*-W392X neonates. (A) Scheme for genetic, biochemical, and safety analysis of P0 *Idua*-W392X neonates injected ICV with C3.MPS LNPs. (B) NGS results at the expected site of base editing in three different sections of harvested brain tissue normalized to negative control (PBS); mean represented by horizontal line for each group. (C) IDUA activity measured after harvest in three different sections of brain tissue from B6 mice (positive control), C3.MPS LNP-treated *Idua*-W392X mice (experimental group), and untreated *Idua*-W392X mice (negative control). (D) GAG amounts in three sections of brain tissue from B6, C3.MPS LNP-treated *Idua*-W392X, and untreated *Idua*-W392X mice. (E) Cytokine analysis in serum of *Idua*-W392X neonates treated 24 h

https://doi.org/10.1021/acsnano.3c02268
ACS Nano XXXX, XXX, XXX−XXX

Figure 4. continued

prior with C3.MPS LNPs. **p < 0.01, ***p < 0.001, ****p < 0.0001 by two-way analysis of variance (ANOVA) with posthoc Šídák's multiple comparisons test; minimum n = 3 per treatment group; error bars represent SEM. (F) Serum anti-PEG IgM antibody levels in neonatal or adult mice 1 week following C3.MPS LNP treatment. *** p < 0.001 by Student's t test with α = 0.05; minimum n = 3 per treatment group; error bars represent SEM. (G) NGS results at the *Idua* on-target site and the top computationally predicted off-target sites in brain genomic DNA of two C3.MPS LNP-treated *Idua*-W392X mice and one PBS-treated negative control. (H) Hematoxylin and eosin (H&E) stained whole brain tissue sections of PBS- or C3.MPS-treated Balb/c neonates with focus on the lateral ventricle. Scale bars: 1 mm (1×) and 50 μm (20×).

the C3 LNP formulation at a 10:1 N:P ratio was selected for further study.

While reporter mRNA was used in the first two phases of *in vitro* optimization to improve throughput, our goal was to deliver CRISPR-base editing mRNA and sgRNA to perinatal brain cells. Thus, we evaluated the feasibility of C3 LNPs to coencapsulate both adenine base editor (ABE7.10) mRNA and an sgRNA specific for the *Idua* G → A (W392X) mutation present in the mouse model of MPS-IH (C3.MPS LNPs).[9] C3 LNPs encapsulating ABE7.10 mRNA and sgRNA at three different mass ratios were formulated and assessed for on-target editing in MPS-IH mouse fibroblasts. A 3:1 ratio of ABE7.10 mRNA:sgRNA within C3 LNPs resulted in the highest level of editing (Figure 3E) and was subsequently used in a dose−response study for on-target editing in MPS-IH mouse neurons and for toxicity studies in MPS-IH mouse fibroblasts and neurons. These studies demonstrated dose-dependent A → G editing of the target adenine in the mouse *Idua* gene (Figure 3F) and no toxicity in either cell type (Figure S8C). Based on these *in vitro* optimization studies, future experimentation was conducted with the C3 LNP at the original formulation parameters, an N:P ratio of 10:1, and an mRNA:sgRNA ratio of 3:1.

C3.MPS LNPs Mediate Biochemical Rescue of Disease in the Neonatal MPS-IH Mouse Brain. We next tested the safety and efficacy of the optimized C3 LNP formulation *in vivo* in a murine model of congenital brain disease (Figure 4A). P0 *Idua*-W392X neonates were injected ICV with C3.MPS LNPs containing 1 mg/kg of RNA and assessed at 1 month of age for on-target editing and amelioration of biochemical manifestations of MPS-IH. PBS injected age- and sex-matched *Idua*-W392X mice and C57Bl/6 (B6) mice served as controls. Next-generation sequencing (NGS) demonstrated low-level on-target base editing at the disease-causing locus in several regions of harvested brain tissue (Figure 4B). Overall editing efficiency in the brain was comparable to that observed previously in the $R26^{mT/mG}$ mouse model. Notably, no editing above baseline was noted in genomic DNA isolated from the liver and gonads (Figure S9), demonstrating similar brain specific delivery observed in our initial LNP library screen. Survival after neonatal ICV injection was 100% in the *IDUA*-W392X neonates.

Next, we explored if durable biochemical corrections existed in the brains of *Idua*-W392X mice treated with C3.MPS LNPs. Similar to patients with MPS-IH, *Idua*-W392X mice have undetectable α-L-iduronidase (IDUA) enzyme activity and elevated tissue glycosaminoglycans (GAGs).[32] At one month, mice treated with C3.MPS LNPs demonstrated increased IDUA activity in the midbrain (p < 0.001, 6.97% of normal) and hippocampus (p < 0.0001, 11.3% of normal) relative to untreated *Idua*-W392X mice that was associated with a reduction in GAG levels in the respective brain regions (Figures 4C and 4D). These data suggest that C3.MPS LNPs facilitate partial biochemical correction of disease in the neonatal *Idua*-W392X mouse brain, demonstrating the potential for mitigation of brain disease in MPS-IH.

C3.MPS LNPs Exhibit Genomic and Immunologic Safety in the Neonatal MPS-IH Mouse. To further study the safety of C3.MPS LNPs, we investigated the acute systemic immune response following LNP treatment. A cohort of *Idua*-W392X mice was injected ICV at P0 with C3.MPS LNPs containing 1 mg/kg of RNA, and serum cytokines were assessed 24 h later. Serum from PBS-injected mice and mice injected with LNPs formulated with MC3 ionizable lipid (MC3.MPS) served as controls. Four pro-inflammatory cytokines, G-CSF (regulator of neutrophil production), IL-1a (driver of inflammation), IP10 (immune cell chemotaxis), and MCP-1 (monocyte migration), were elevated in C3.MPS LNP- and MC3.MPS-treated neonates compared to PBS-treated controls (Figure 4E). Furthermore, MC3.MPS LNP-treated mice demonstrated a significant increase in serum IP10, IL-9 (pleiotropic cytokine with both pro- and anti-inflammatory function), and GM-CSF (regulator of macrophage production) levels relative to mice treated with C3.MPS LNPs. Taken together, these data suggest that while C3.MPS LNPs do produce an acute serum cytokine response that is generally pro-inflammatory, this reaction is at a lower level than that produced by FDA-approved MC3 LNPs.

Recent studies have revealed that PEGylated therapies give rise to anti-PEG antibodies in animal models and patients.[33] While PEGylation of LNPs attracts a water shell, reducing adsorption of opsonins and evading recognition of LNPs by the mononuclear phagocyte system, antibodies to PEG-lipid may cause adverse immune effects, reduce therapeutic efficacy, and limit the potential for repeat dosing due to the accelerated blood clearance phenomenon.[34] To characterize the anti-PEG antibody response elicited by C3.MPS LNPs, P0 *Idua*-W392X mice were injected ICV, and the serum was assessed 1 week later for anti-PEG IgM antibodies. No significant difference in anti-PEG IgM levels was observed between C3.MPS LNP-treated and PBS-treated neonates. In contrast, a 2.5-fold increase in serum anti-PEG IgM antibodies in C3.MPS LNP-treated adult mice compared to PBS-treated adult mice (p < 0.001) was observed (Figure 4F). These data are consistent with our previous study demonstrating that the immune system of a P0 mouse is immature[35]—similar to that of a developing human fetus—and imply that a mature immune system, as is present in an adult mouse, is capable of producing an anti-PEG IgM response to C3.MPS LNPs.

Next, we investigated the genomic safety of our LNP-mediated base editing strategy. Next-generation sequencing of brain genomic DNA from experimental mice did not demonstrate off-target base editing above background at nine previously identified possible off-target sites for the sgRNA targeting the mouse *Idua* G → A mutation were assessed by NGS (Figure 4G).[9] Finally, we assessed the potential toxicity

https://doi.org/10.1021/acsnano.3c02268
ACS Nano XXXX, XXX, XXX−XXX

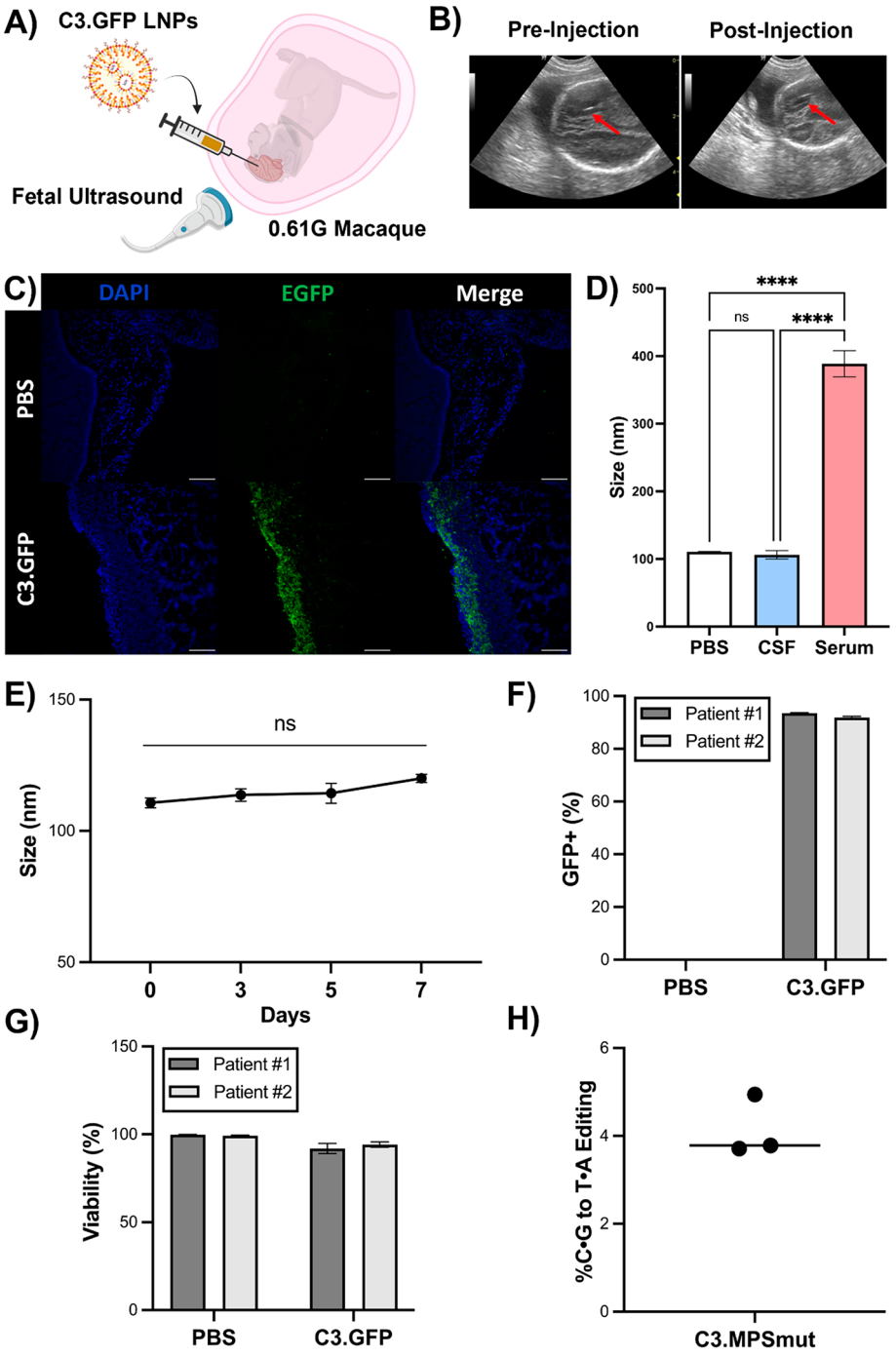

Figure 5. | C3 LNP-mediated *in utero* mRNA delivery to the NHP brain and *ex vivo* performance in pediatric biological fluids and brain tissue. (A) Experimental scheme depicting ultrasound guided ICV injection of C3 LNP.GFP in a 0.61G *Macaca fascicularis*. (B) Ultrasound images (red arrow points to needle) pre- and post-ICV injection of C3.GFP LNPs in fetal macaque. (C) GFP immunohistochemistry on brain sections from C3 LNP.GFP-treated and negative control animals. Scale bars: 100 μm (10×). (D) Size and PDI measurements of C3.MPS LNPs incubated in PBS, human CSF, or human serum. ****$p < 0.0001$ by one-way ANOVA with Tukey's multiple comparisons test. (E) Size measurements of C3.MPS LNPs incubated in human CSF over a 7-day time course. (F) GFP positivity in two patient-derived primary cell lines enriched for neurons after C3.GFP LNP treatment. (G) Viability after C3.GFP LNP treatment in both patient-derived cell lines. (H) NGS results in patient-derived precision cut brain slices treated with C3.MPS LNPs normalized to control (PBS). Outliers were detected using Grubbs' test and removed from analysis; minimum $n = 3$ per treatment group; error bars represent SEM.

of C3.MPS LNPs in P0 Balb/c neonates via brain hemotoxin and eosin (H&E) staining (Figure 4H). Relative to PBS-treated brain tissue sections, there was no evidence of gross structural damage or inflammatory cell infiltration near the injection site in the LNP-treated brains.

C3 LNPs Enable mRNA Delivery to Cerebral Ventricular Cells in a Fetal Macaque. We next evaluated the feasibility of C3 LNP-mediated mRNA delivery to the brain in a fetal large animal model. Relative to fetal and neonatal mouse models, nonhuman primate models have more structurally similar brain anatomy to humans and allow for the

https://doi.org/10.1021/acsnano.3c02268
ACS Nano XXXX, XXX, XXX−XXX

evaluation of delivery platforms via a minimally invasive, ultrasound-guided ICV injection, that would be used clinically. Thus, we evaluated the translational potential of our delivery platform in a 0.61G *Macaca fascicularis*, a gestational age that approximates the developmental stage of a midgestation human fetus when therapeutic intervention is clinically feasible.

C3 LNPs encapsulating GFP mRNA (C3.GFP) were administered ICV via transabdominal ultrasound guidance at a dose of 1 mg/kg into the lateral ventricle of a 0.61G macaque (Figure 5A). Successful delivery was confirmed by the observation of transient ventricular swelling (Figure 5B). Then, 48 h after injection, the fetus was delivered by caesarian section and GFP expression in the brain was assessed by immunohistochemistry. Tissue sections of harvested fetal macaque brain demonstrated strong GFP expression in the cells lining the lateral ventricles, similar to the region transfected in our previous $R26^{mT/mG}$ mouse studies (Figure 5C). This result demonstrates that the mRNA delivery performance of C3 LNPs in the perinatal brain translates to a larger scale animal model more developmentally similar to a human, while highlighting the need for future optimization to enhance targeting deeper regions of the nonhuman primate brain.

LNPs Demonstrate Translational Potential in Patient-Derived Brain Tissues. To further evaluate the potential clinical relevance of C3 LNPs for mRNA delivery to the human brain, we tested their performance in three patient-derived samples—cerebrospinal fluid (CSF), neurons derived from brain tissue, and precision-cut three-dimensional brain slices. We previously developed an assay to evaluate LNP stability in fetal fluids and demonstrated that *ex vivo* stability predicts *in vivo* mRNA delivery.[28] As such, C3.MPS LNPs were incubated in pediatric cerebrospinal fluid (CSF), the fluid into which they would be clinically delivered, and assessed for stability via size and charge measurements (Figure 5D and Figure S10). No significant change in size or polydispersity of C3.MPS LNPs incubated in human CSF was observed (Figure 5D), and this result was confirmed over a 1 week time course, supporting the stability of our LNP (Figure 5E). In contrast, incubation of C3.MPS LNPs in human serum resulted in significant aggregation and clustering (Figure 5D). Previous studies have reported that LNP zeta potential measurements become more negative at increasing concentrations of protein-rich fluid.[28] However, the zeta potential of C3.MPS LNPs did not change at increasing concentrations of human CSF (Figure S10C), implying that these LNPs avoid significant protein adhesion that can reduce cellular uptake.

Next, neurons were cultured from the cerebral cortex tissue of two pediatric patients undergoing neurosurgical procedures. C3.GFP LNPs resulted in a high transfection efficiency (Figure 5F) with no significant effect on viability (Figure 5G) of these cells. We then sought to demonstrate C3 LNP-mediated base editing in human brain tissue. Using an established protocol,[36] precision cut slices of pediatric brain tissue were generated and cultured *ex vivo* in a 50:50 mixture of human CSF and serum-free media. C3 LNPs (C3.MPSmut LNPs) encapsulating cytosine base editor (BE3) mRNA and an sgRNA to introduce a C → T mutation (W402X) in the *IDUA* gene—a common mutation in MPS-IH patients—were applied to precision cut brain slices. NGS demonstrated ~4% on-target editing (Figure 5H) supporting the ability of C3 LNPs to codeliver a functional base editor mRNA and sgRNA in an *ex vivo* human brain tissue model.

DISCUSSION

Most genetic brain diseases lack reasonably effective therapies due to the complexity of the CNS, the limited regenerative capacity of the tissue, and the difficulty of therapeutics crossing the blood–brain barrier.[37] Since congenital brain pathology often begins before birth, fetal intervention provides a therapeutic opportunity to mitigate irreversible disease burden.[3] Through correction of underlying pathogenic mutations, gene editing technologies offer a potential curative strategy for genetic diseases with CNS features after a single treatment. However, the applicability of gene editing therapies in the perinatal CNS is currently limited by the lack of a safe and effective nucleic acid delivery platform. Here, we screen a diverse ionizable LNP library for delivery of mRNA to the murine fetal and neonatal CNS and demonstrate LNP-mediated base editing and partial biochemical correction of disease after *in vitro* optimization of the lead LNP platform. In addition, we achieve LNP-mediated mRNA delivery to the CNS of a fetal NHP *in vivo* and characterize the stability and base editing performance of our optimized LNP *ex vivo* in patient-derived human brain tissues. This proof-of-concept study supports the safety and efficacy of LNPs for the delivery of mRNA-based gene editing therapies to the CNS.

In this work, a mouse model of MPS-IH was chosen to study LNP-mediated perinatal delivery of a gene editing therapy since the neurodevelopmental pathology in patients with this disease starts prior to or shortly after birth, is irreversible, and is resistant to currently available treatments, including enzyme replacement therapy and hematopoietic stem cell transplant.[9] MPS-IH is caused by genetic mutations in the *IDUA* gene, resulting in IDUA enzyme deficiency. One of the most common *IDUA* disease-causing mutations is amenable to correction by adenine base editing resulting in restoration of IDUA enzyme activity and improvement in disease pathology including the reduction in lysosomal accumulation of GAGs.[9] Despite low-level LNP-mediated adenine base editing at the pathogenic locus in the neonatal MPS-IH mouse brain, we observed a partial restoration of IDUA enzyme activity (7–11% of normal) and a reduction in the accumulation of GAGs in multiple brain regions. We previously demonstrated stable editing in multiple organs from 1 month to 6 months after *in utero* AAV-mediated adenine base editing in the MPS-IH mouse model.[9] Similarly, future studies investigating the long-term stability of both C3 LNP-mediated base edits and biochemical correction as treated animals grow from neonates to adults are important. However, since studies suggest that 1% of normal IDUA enzyme activity may be sufficient to transition from severe Hurler's syndrome to the milder Scheie syndrome,[38] the low-level editing observed via the current approach may beneficially affect the neurobehavioral phenotype in MPS-IH, although assessment of this outcome is limited in the current study due to the lack of a strong neurobehavioral phenotype in this mouse model at the short time points assessed.[9] The improvement in IDUA and GAG levels is likely due to secretion of the IDUA enzyme into the CNS by a small number of corrected periventricular cells, which is supported by our studies in neonatal reporter mice demonstrating the predominance of editing confined to periventricular cells after intraventricular injection of LNPs. Thus, while the lead LNP engineered in this study holds promise for CNS diseases in which a paracrine effect of restoring normal protein function following periventricular cell

https://doi.org/10.1021/acsnano.3c02268
ACS Nano XXXX, XXX, XXX–XXX

targeting is adequate, further LNP optimization is required to apply this delivery modality to a broader range of diseases involving nonperiventricular structures or specific neural cell types.

Engineering of LNPs is an iterative process, and characterization of our lead LNP has established critical parameters for LNP-mediated nucleic acid delivery to the perinatal CNS. LNPs containing the C3 ionizable lipid were small (<100 nm), monodisperse (<0.20 PDI), and well-encapsulated (>90%) and were on the lower end of the known pK_a range (~5) for efficient mRNA delivery. Given the more acidic pH of CSF and size of intercellular junctions adjoining brain cell types,[39] we hypothesize that these parameters convey better *in vivo* efficacy in the perinatal brain. More broadly, the trends observed for *in vivo* transfection efficiency of our LNP library in the fetal mouse brain matched those seen in the neonatal mouse brain, validating that the neonatal mouse model can be used to approximate LNP performance in the fetal mouse CNS. Importantly, the top-performing LNP following *in utero* ICV mRNA delivery was in the bottom quartile of LNPs for targeting the fetal liver following *in utero* intravascular mRNA delivery.[19] These findings highlight the variability of cell-type-specific *in vivo* LNP targeting dependent on LNP characteristics. In addition to the identity of the ionizable lipid, a range of variables during LNP formulation are known to influence the *in vivo* delivery of gene editing platforms. We assessed several of these variables *in vitro* in neuronal origin cells. Modulation of the LNP lipid ratio parameters suggested that our original LNP formulation mediated efficient mRNA delivery. An optimal weight ratio of base editor mRNA to sgRNA within the lead LNP formulation (3:1) was also identified, differing from previous reports of LNPs coencapsulating base editor mRNA and sgRNA.[16,40] Further strategies to improve LNP-mediated gene editing include *in vivo* screening of a large DOE library of LNPs via mRNA barcoding, optimization of mRNA cargo modifications, or addition of cell-specific targeting moieties to the LNP surface.

Highly effective "traditional" replacement gene therapy to the perinatal CNS has previously been achieved in several animal studies via viral vectors. For instance, Waddington and colleagues utilized AAV9 to rescue a mouse model of Gaucher's disease and demonstrated brain transduction following ICV administration of AAV9 in the fetal NHP model.[41] While AAVs were shown to be effective for these applications, recent concern over AAV toxicity at high doses motivates the development of nonviral alternatives.[42] This is especially important when considering fetal gene therapy or gene editing in which the fetus may be more prone to toxicities of the delivery vehicle, and the mother, who, in most cases, is unaffected by the disease, must not be harmed. In this study, C3 LNPs did not result in morphological changes to the fetal or neonatal murine brain parenchyma on gross examination. In addition, the ICV delivery of C3 LNPs encapsulating a base editing platform to treat the mouse model of MPS-IH did not result in demonstrable editing in the liver and gonads. Thus, while this delivery modality holds promise for the CNS pathology of MPS-IH and other genetic diseases limited to CNS pathology, diseases with multiorgan pathology would require additional systemic delivery approaches for complete treatment.

Assessment of the acute serum cytokine response following C3 LNP treatment of MPS-IH neonates exhibited elevated levels of a small subset of cytokines; however, this response was lower than that produced by FDA-approved LNPs encapsulating the same base editing platform. ICV administration of C3 LNPs in the mouse neonate, which immunologically mimics a mid- to late-gestation human fetus, also did not elicit an anti-PEG IgM antibody response, in contrast to that seen following injection of the same LNPs in the adult mouse brain. These results highlight the opportunity for repeat LNP injections to boost longitudinal therapeutic efficacy.[18] While these results coupled with our survival data in neonatal mice, brain tissue histology, and off-target genomic analysis are encouraging, additional safety analyses of our LNP base editing platform are required prior to translation, including unbiased genomic off-target analyses, long-term anti-PEG IgG responses, immune responses to repeat doses of an LNP-based therapeutic, and evaluation of long-term systemic organ toxicity.

Although valuable insights can be gained from *in vitro* and *in vivo* small animal studies, testing delivery carriers in models that better account for the size, complexity, and species variability of the human CNS is critical for consideration of clinical translation.[42] To this end, we evaluated the ability of C3 LNPs to deliver mRNA to the fetal brain in the NHP via ICV administration at a gestational age akin to a midgestation human fetus and demonstrated transfection of the brain ventricular lining akin to our studies in the mouse model. In addition, given the ultimate goal of developing an LNP platform for delivery into the CSF-filled ventricles of patients, we assessed the stability of C3 LNPs in human CSF and demonstrated that LNPs retained their physiochemical properties upon incubation in CSF but not human serum *ex vivo*. Prior studies have demonstrated that the molecular composition of an LNP modulates the endogenous proteins that bind the nanoparticle and govern its biological fate.[43] Both the abundance and identity of proteins in the CSF are distinct relative to the serum,[44] which may contribute to the difference in stability, and subsequently performance, of LNPs in these two biological fluids. Proteomics-based identification of specific proteins that bind C3 LNPs in the CSF in future studies may allow for enhanced LNP-mediated cellular uptake in the perinatal brain through receptor targeting. Finally, we generated precision-cut slices of human cortical brain tissue and demonstrated C3 LNP-mediated base editing of the gene implicated in MPS-IH. Taken together, these experiments provide the foundation for additional translational studies and demonstrate base editing facilitated by a nonviral delivery carrier in the NHP fetal brain and primary human brain tissue.

CONCLUSIONS

Delivery of mRNA-based therapeutics to the perinatal brain holds great potential in treating congenital brain disorders with limited therapeutic options. Although previous work has evaluated virally mediated gene delivery to the CNS, nonviral mediated delivery of mRNA therapeutics to the CNS has been less robustly studied and offers potential safety advantages over viral vector delivery approaches. Here, we engineer an LNP platform to begin to address this need, demonstrating its efficacy and safety in a mouse model of a human disease, in the fetal NHP model, and in patient-derived brain tissues. With future optimization, these LNPs may offer a translatable delivery platform for *in utero* and neonatal CNS-directed gene editing.

https://doi.org/10.1021/acsnano.3c02268
ACS Nano XXXX, XXX, XXX−XXX

MATERIALS AND METHODS

Ionizable Lipid Synthesis. Ionizable lipids were prepared via Michael addition chemistry as previously described.[20] Epoxide-terminated alkyl chains (Avanti Polar Lipids) were reacted with polyamine cores (Enamine Incorporated). The components were combined at an excess of lipid epoxides in a 4 mL amber vial with a magnetic stir bar. The crude product was transferred to a Rotavapor R-300 instrument (BUCHI) for solvent evaporation, and the lipids were suspended in ethanol for use.

mRNA Synthesis and Production. mRNA was produced by using standard *in vitro* transcription methods. Luciferase, GFP, ABE7.10, and BE3 gene sequences were codon optimized and cloned into proprietary mRNA production plasmids. The m1Ψ UTP nucleoside modified mRNA was cotranscriptionally capped with a trinucleotide cap1 analogue (TriLink) and engineered to contain a 101 nucleotide-long poly(A) tail. Transcription was performed using MegaScript T7 RNA polymerase (Invitrogen), and mRNA was precipitated before purification via cellulose chromatography. mRNAs were analyzed by agarose gel electrophoresis, sequenced, subjected to a standard J2 dot blot, assayed for INF induction in human monocyte derived dendritic cells, and stored at −80 °C.

Cre recombinase mRNA fully substituted with 5-methoxyuridine was sourced from TriLink Biotechnologies via the CleanCap platform. sgRNAs were sourced from Integrated DNA Technologies via the Alt-R platform. The mouse *Idua* gene targeting protospacer and PAM was 5′-ACTCTAGGCAGAGGTCTCAA|AGG-3′ as described in our previous work.[9] The protospacer and PAM to introduce the most common mutation in the W402X human *Idua* gene was 5′-CCAGAGCTGCTCCTCATCTG|CGG-3′.

LNP Formulation. Ionizable lipids, prepared as described above, or DLin-MC3-DMA (MedChem Express) were combined in an ethanol phase with cholesterol (Sigma-Aldrich), DOPE (Avanti), and 1,2-dimyristoyl-*sn*-glycero-3-phosphoethanolamine-*N*-[methoxy-(polyethylene glycol)-2000] (C14-PEG2000, Avanti) at a molar ratio of 35:46.5:16:2.5 or at molar ratios specified in Figure S6. An aqueous phase was prepared consisting of 25 μg of *luciferase* mRNA, 25 μg of GFP mRNA, or 25 μg of total mRNA at a variable mass ratio of ABE to sgRNA in 10 mM citrate buffer (pH 3). The ethanol and aqueous phases were then combined at a 3:1 ratio through channels in a microfluidic device facilitated by a Pump33DS syringe pump (Harvard Instruments) or rapidly mixed and incubated. LNPs were dialyzed against 1X PBS for 2 h before sterile filtration via 0.22 μM filters. All materials were prepared and handled ribonuclease-free.

LNP Characterization. Zetasizer Nano (Malvern Instruments) was used to measure the diameter (*z*-average) and polydispersity index (PDI) of LNPs suspended in 1X PBS at a dilution factor of 1 to 100. Zeta potential measurements were collected for LNPs suspended in deionized water at a dilution factor of 1 to 100 using the Zetasizer Nano and DTS1070 zeta potential cuvettes (Malvern Panalytical).

pK_a measurements were conducted as previously described.[22] Buffered solutions of 150 mM sodium chloride, 20 mM sodium phosphate, 20 mM ammonium acetate, and 25 mM ammonium citrate were each adjusted to pH 2 to 12 in increments of 0.5. Then, 200 μL of each pH-adjusted solution was combined with 5 μL of each LNP formulation. TNS [6-(*p*-toluidinyl)naphthalene-2-sulfonic acid] was added to each well at a final TNS concentration of 6 μM. Fluorescence intensity was read on an Infinite 200 Pro plate reader (Tecan), and pK_a was calculated as the pH at which the fluorescence intensity was 50% of its maximum value, reflective of 50% protonation.

Encapsulation efficiencies were calculated using Quant-iT RiboGreen (Thermo Fisher Scientific) assay as previously described.[19] Equal concentrations of LNPs were treated with either Triton X-100 (Sigma-Aldrich) or left untreated, and after incubation, the groups were plated alongside RNA standards. RiboGreen reagent was added, and fluorescence was measured on a plate reader at an absorbance range of 480 nm/520 nm. A standard curve was generated by using RNA standards and used to quantify RNA content and calculate encapsulation efficiency.

Animal Experiments. All mouse animal protocols were approved by the Institutional Animal Care and Use Committee (IACUC) at Children's Hospital of Philadelphia (IACUC 21-001417) and followed the guidelines in the NIH's Guide for the Care and Use of Laboratory Animals.

BALB/c, B6.129(Cg)-Gt(ROSA)26Sor$^{tm4(ACTB-tdTomato,-EGFP)Luo}$/J (*R26*^{mTmG}), and B6.126S-*Idua*$^{tm1.1Kmke}$/J (*Idua*-W392X) were purchased from Jackson Laboratory (Bar Harbor, ME). Mice were housed in the Laboratory Animal Facility at Children's Hospital of Philadelphia.

Macaque procedures were performed in accordance with IACUC at the National University of Singapore and Singapore Health Services (IACUC 2009-SHS-512). The macaque experiments were conducted at the SingHealth Experimental Medicine Centre, accredited by the Association for Assessment and Accreditation of Laboratory Animal Care International.

Mouse ICV Injection. *In utero*, neonatal, and adult bilateral ICV injection were performed as described previously.[41,45,46] *Fetus*: 18-day gestation BALB/c fetuses were used to screen the LNP library *in vivo*. Briefly, under isoflurane anesthesia, a maternal midline laparotomy was performed to expose the uterine horns. Either 4 μL of PBS or LNPs containing 1 mg/kg mRNA was injected into the lateral ventricles using an 80 μm beveled glass micropipette and a Narishige IM-400 Electric Microinjector (Narishige International). After successful injection, confirmed by visualizing clearance of the injectate and transient swelling of the ventricle, the uterus was returned to the peritoneal cavity, the abdomen was closed, and the mice recovered in a warm cage. *Neonate*: P0 BALB/c or *Idua*-W392X pups were anesthetized on ice, and 4 μL of PBS or LNPs containing 1 mg/kg mRNA was injected into the lateral ventricles under a dissecting microscope using an 80-μm beveled glass micropipette and automated microinjector. After successful injection, pups were recovered on a warming pad and returned to a nursing foster mother. *Adult*: After appropriate analgesia and isoflurane anesthesia, a 31-guage needle was used to penetrate the skull and access the lateral ventricles in 12-week-old BALB/c mice. Ten microliters of either PBS or LNPs containing 1 mg/kg mRNA was injected. Following injection, skin was closed with running 5−0 absorbable sutures, and animals recovered.

Luciferase Imaging. Mice were imaged 4 h after injection with LNPs on an *in vivo* imaging system (IVIS, PerkinElmer). Prior to imaging, animals were injected intraperitoneally with D-luciferin (150 mg/kg) and potassium salt (Biotium). After sacrifice, whole specimens or dissected organs were imaged via IVIS, and luminescence signal was detected with a standardized exposure time. Image analysis was conducted in the Living Image software (PerkinElmer). To quantify luminescent flux, a rectangular ROI was placed over each sample, and an ROI of the same size was placed in an area without any luminescent signal in the same image. Normalized flux was calculated by dividing total flux from the sample area by the total flux from the background area.

R26$^{mT/mG}$ and Balb/c Mouse Studies and Brain Immunohistochemistry. P0 R26$^{mT/mG}$ neonates were injected ICV with either PBS or C3 LNP. One week after injection, animals were harvested by standard transcardiac perfusion using 4% PFA followed by overnight fixation. After 24 h, samples were transferred to 30% sucrose for cryoprotection. Tissues were embedded in the OCT compound and sectioned on a cryostat. Sections were mounted on Superfrost Plus slides (Thermo Fisher Scientific) and frozen at −80 °C.

For immunostaining, slides were dried at 60 °C via a slide warmer and rehydrated in 1X PBS. Tissues were blocked with 10% donkey serum (Sigma-Aldrich) followed by overnight incubation with 1:500 dilutions of the following primary antibodies: NeuN (Rabbit mAb #12943, Cell Signaling Technology), IBA1 (Rabbit mAb 019-19741, FUJIFILM Wako Pure Chemical Corporation), and GFAP (Rabbit mAb GA524, Agilent Technologies). After 24 h, slides were washed with 1X PBS and incubated with Alexa Fluor-conjugated secondary antibodies for 2 h at room temperature. Slides were mounted on Fluoroshield Mounting Medium with DAPI (Abcam) and imaged on a fluorescence microscope (BZ-X, Keyence). A similar protocol was executed for immunostaining of sectioned Balb/c neonatal brain

https://doi.org/10.1021/acsnano.3c02268
ACS Nano XXXX, XXX, XXX−XXX

tissue for H&E via the Hematoxylin and Eosin Staining Kit (ab245880).

***In Vitro* LNP Optimization Studies.** Neuro-2a cells (ATCC CCL-131) were cultured in Dulbecco's Modified Eagle's Medium (DMEM) with *l*-glutamine (Thermo Fisher Scientific) supplemented with 10% fetal bovine serum (FBS) (Gibco) and 1% penicillin–streptomycin (Gibco). Cells were plated at a density of 1000 cells/μL, incubated overnight, and dosed with LNPs encapsulating 100 ng of GFP mRNA in serum-free media. After 24 h, cells were detached via trypsin, washed with 1X PBS, and resuspended in flow cytometry (FACS) buffer (Ca^{2+}/Mg^{2+} Free PBS, 0.5% BSA, 0.5 mM EDTA). Samples were analyzed for fluorescence via flow cytometry (BD FACSAria Cell Sorter) for GFP+. Viability was assessed via a Live/Dead Cytotoxicity Kit (Thermo Fisher Scientific).

Primary fibroblasts or primary neurons were harvested from an adult *Idua*-W392X mouse. The mouse was euthanized, and organ tissue was isolated prior to mechanical digestion and filtering through 100 μm cell strainers. Cells were washed with 1X PBS and subsequently cultured in DMEM supplemented with 15% FBS and 1% penicillin–streptomycin. Either primary fibroblasts or primary neurons were plated at a cellular density of 1000 cells/μL, incubated overnight, and treated with LNPs at a range of ABE to sgRNA ratios and doses in serum-free media. After 5 days, cells were detached via trypsin, washed in 1X PBS, and resuspended in QuickExtract DNA Extraction Solution (Lucigen Corporation). Q5 polymerase was used to amplify the genomic region encompassing the W392X mutation with the following primers (F, 5′-TGCTAGGTATGAGAGAGCCA-3′; R, 5′-AGTGTAGATGAGGACTGTGGT-3′) at an annealing temperature of 66 °C. PCR products were evaluated using an agarose gel, purified using a Qiagen PCR Purification Kit, and analyzed by Sanger sequencing (Azenta Life Sciences).

***Idua*-W392X Mouse Studies (On- and Off-Target Editing, IDUA Activity, Tissue GAG Assay).** P0 *Idua*-W392X neonates were injected ICV with C3.MPS LNPs containing 1 mg/kg total mRNA. Untreated *Idua*-W392X mice and wild-type B6 mice served as positive and negative controls. After one month, animals were sacrificed, and brain tissue (forebrain, midbrain, hippocampus), liver, and gonads was harvested. DNA was extracted using the Qiagen DNEasy Blood and Tissue Kit (Qiagen), PCR amplified, purified, and analyzed via NGS (Azenta Life Sciences).

The top ten off target sites were predicted using CRISPOR and ranked using the Cutting Frequency Determination off-target score. These sites were PCR amplified using Platinum SuperFi II Hi-Fidelity DNA Polymerase (Thermo Fisher Scientific), PCR amplified and purified, and analyzed via NGS (Azenta Life Sciences).

Tissue IDUA activity was assayed as described previously.[9] Tissue samples were homogenized with 0.1% Triton X-100 lysis buffer using a TissueLyser LT (Qiagen). IDUA enzyme activity was induced using 4-methyl-umbelliferyl-α-L-iduronide (Glycosynth). After incubation, reactions were arrested using glycine carbonate buffer, and fluorescence was measured via a plate reader. Enzyme activity was normalized to sample protein content measured via a Pierce BCA Protein Assay Kit (Thermo Fisher Scientific). After obtaining IDUA enzyme activity, 0.5 mL of papain solution (Sigma-Aldrich) was added to homogenized tissue lysates. Samples were incubated at 65 °C for 3 h and centrifuged to clarify supernatant. Total sulfated GAG content in each sample was assessed using the Blyscan Glycosaminoglycan Assay (Biocolour). Tissue GAG content was normalized to the sample protein content.

***Idua*-W392X Mouse Studies (Cytokine Analysis, Anti-PEG IgM Antibody).** P0 *Idua*-W392X were injected ICV with either 1X PBS or C3.MPS/MC3.MPS LNPs containing 1 mg/kg total mRNA. Animals were bled after 24 h prior to analysis via 25-proinflammatory cytokine panel (MilliporeSigma). A standard curve for each plate was prepared by serial dilution of the provided standards in the appropriate dilutant. Multiplex plates were run on a MAGPIX system (Luminex Corporation). Each cytokine was assessed using a five-parameter regression algorithm and normalized to sample protein concentration determined by microBCA assay.

P0 *Idua*-W392X neonates and adults were injected ICV with either PBS or C3.MPS containing 1 mg/kg total mRNA. Animals were bled after 7 days, and the concentration of circulating IgM anti-PEG antibodies was assessed by Mouse Anti-PEG IgM ELISA (Life Diagnostics Incorporated). Concentration of IgM anti-PEG antibody was calculated based on a standard curve.

LNP Administration to Fetal Macaque and Brain Immunohistochemistry. A cynomolgus macaque (*Macaca fasicularis*) was used for a proof-of-principle nonhuman primate (NHP) study. Macaques underwent timed mating with pregnancy confirmed through ultrasound evidence of a fetal pole and fetal heart activity. Dating was performed as previously reported,[41] and *in utero* ICV injection was performed at 0.61G. In brief, anesthesia was induced via sevoflurane. A 25G Quincke needle (Becton-Dickenson) was used to target the lateral ventricle closest to the anterior maternal abdomen under continuous ultrasound imaging. C3 LNP containing 1 mg/kg total mRNA was injected as a slow bolus, and transient ventricular swelling validated successful delivery. The needle was removed, and both mother and fetus were monitored postoperatively. Animals were sacrificed after 48 h, and macaque brains were harvested using isoflurane and pentobarbitone, cardiac puncture, and perfusion of 1% PFA.

After 24 h, samples were cryoprotected, embedded in an OCT compound, sectioned, and mounted on Superfrost Plus slides (Thermo Fisher Scientific). For immunostaining, slides were dried at 60 °C via a slide warmer and rehydrated in 1X PBS. Tissues were blocked with 10% donkey serum (Sigma-Aldrich) and incubated overnight with 1:100 dilution of GFP antibody (Rabbit mAb ab290). After 24 h, slides were washed with 1X PBS, incubated with an Alexa Fluor-conjugated secondary antibody for 2 h at room temperature, and mounted on Fluoroshield Mounting Medium with DAPI prior to imaging.

LNP Stability in Human Fluids. All human specimens were collected following the Institutional Review Board (IRB) approval at the Children's Hospital of Philadelphia (IRB 21-018470). LNP stability in patient-derived fluids was assessed via our previously published protocol.[28] In brief, C3.MPS LNPs were incubated in a range of human serum or CSF percentages—0%, 25%, 50%, 75%, 90% and 100% (volume biological fluid/total sample volume) for 30 min at 37 °C under gentle agitation. After 30 min, each sample was diluted 1 to 100 in 1X PBS and transferred to a standard cuvette for size, PDI, or zeta potential measurement via Zetasizer Nano.

Isolation of Patient-Derived Precision Cut Brain Slices and Brain Cells. Brain tissue was dissected and transferred into ice-cold patient cerebrospinal fluid equilibrated with carbogen (95% O_2, 5% CO_2). Tissue was trimmed, and 300 μm slices were prepared using a vibratome (Leica Biosystems). Slices were transferred to tissue culture plates and cultured in media modified from prior protocols:[36] 50% DMEM, 48% Neurobasal Media (Thermo Fisher Scientific), 1X GlutaMAX (Gibco), and 20 mM HEPES (Thermo Fisher Scientific).

Primary human brain cells were isolated via an established protocol.[47] Patient-derived brain tissue was mechanically dissociated before enzymatic digestion in papain and DNase I (Invitrogen Corporation) for 30 min at 37 °C. Cell suspension was passed through a 100 μm cell strainer, centrifuged, and resuspended in the media described above. Cells were plated onto poly-D-lysine-coated cell culture surfaces, and 50% of culture media was exchanged every 48 h.

LNP Studies in Patient-Derived Cells and Tissue. Patient-derived primary cells were seeded at a cellular density of 1000 cells/μL in a poly-D-lysine coated 96-well plate and allowed to incubate overnight. Cells were treated with either PBS or C3 LNPs containing 100 ng of GFP mRNA. After 24 h, cells were detached, washed with 1X PBS, and resuspended in FACS buffer. Samples were analyzed for fluorescence (GFP+) via flow cytometry and viability via Live/Dead Cytotoxicity Kit (Thermo Fisher Scientific).

Prior to treatment, precision cut brain slices were cultured in 50% primary brain medium and 50% human CSF. Slices were treated with either PBS or C3.MPSmut LNPs containing 500 ng of total mRNA in serum-free media. After 5 days, slices were mechanically digested,

https://doi.org/10.1021/acsnano.3c02268
ACS Nano XXXX, XXX, XXX–XXX

passed through a 100 μm cell strainer, and resuspended in QuickExtract DNA extraction solution. The genomic region encompassing the human W402X mutation was amplified with KAPA HiFi DNA Polymerase (Roche, Basel, Switzerland) using the following primers (F, 5′-CAATGCCTTCCTGAGCTACCAC-3′; R, 5′-AGGTAGCGCGTGACGTAGAC-3′) at an annealing temperature of 57 °C. PCR products were evaluated using an agarose gel, purified using the Qiagen PCR Purification Kit, and analyzed by NGS (Azenta Life Sciences).

Statistical Analysis. All quantifications represent the mean and standard error of the mean (SEM) acquired from at least three biological replicates (cells or animals) per treatment group. Means were compared via one-way ANOVA with posthoc Dunnett's test, two-way ANOVA with posthoc Šidák's multiple comparisons test, or Student's *t* test. For all experiments, outliers were detected using Grubbs' test and removed from analysis.

ASSOCIATED CONTENT

Data Availability Statement

All data needed to evaluate the conclusions in the paper are present within the main text and/or the Supporting Information. All data and materials are stored at the University of Pennsylvania and Children's Hospital of Philadelphia facilities in the Mitchell and Peranteau laboratories. Additional data may be requested from the co-corresponding authors: M.J.M. (mjmitch@seas.upenn.edu) and/or W.H.P. (peranteauw@chop.edu).

Supporting Information

The Supporting Information is available free of charge at https://pubs.acs.org/doi/10.1021/acsnano.3c02268.

Table with the physiochemical properties of the LNP library; LNP-mediated luciferase expression and N2A cell viability after treatment at three different time points; the relationship between LNP library physiochemical properties and LNP fetal mouse brain transfection efficacy *in vivo*; LNP-mediated luciferase expression in the fetal mouse liver; biodistribution of lead LNP in the fetal mouse after ICV injection; flow cytometry data showing subpopulations of gene modulated brain cells; table displaying range of excipient molar ratios tested in DOE library; impact trend curves from *in vitro* DOE screen; viability after treatment of LNPs from *in vitro* optimization scheme; absence of LNP-mediated base editing in the gonads and liver; and characterization of LNP stability in human CSF and human serum (PDF)

AUTHOR INFORMATION

Corresponding Authors

Michael J. Mitchell − *Department of Bioengineering, University of Pennsylvania, Philadelphia, Pennsylvania 19104, United States; Abramson Cancer Center, Perelman School of Medicine, University of Pennsylvania, Philadelphia, Pennsylvania 19104, United States; Institute for Immunology, Perelman School of Medicine, University of Pennsylvania, Philadelphia, Pennsylvania 19104, United States; Cardiovascular Institute, Perelman School of Medicine, University of Pennsylvania, Philadelphia, Pennsylvania 19104, United States; Institute for Regenerative Medicine, Perelman School of Medicine, Philadelphia, Pennsylvania 19104, United States;* orcid.org/0000-0002-3628-2244; Email: mjmitch@seas.upenn.edu

William H. Peranteau − *Center for Fetal Research, Children's Hospital of Philadelphia, Philadelphia, Pennsylvania 19104, United States; Division of General, Thoracic, and Fetal Surgery, Children's Hospital of Philadelphia, Philadelphia, Pennsylvania 19104, United States*; Email: peranteauw@chop.edu

Authors

Rohan Palanki − *Department of Bioengineering, University of Pennsylvania, Philadelphia, Pennsylvania 19104, United States; Center for Fetal Research, Children's Hospital of Philadelphia, Philadelphia, Pennsylvania 19104, United States;* orcid.org/0000-0001-5168-5634

Sourav K. Bose − *Center for Fetal Research, Children's Hospital of Philadelphia, Philadelphia, Pennsylvania 19104, United States*

Apeksha Dave − *Center for Fetal Research, Children's Hospital of Philadelphia, Philadelphia, Pennsylvania 19104, United States*

Brandon M. White − *Center for Fetal Research, Children's Hospital of Philadelphia, Philadelphia, Pennsylvania 19104, United States*

Cara Berkowitz − *Center for Fetal Research, Children's Hospital of Philadelphia, Philadelphia, Pennsylvania 19104, United States*

Valerie Luks − *Center for Fetal Research, Children's Hospital of Philadelphia, Philadelphia, Pennsylvania 19104, United States*

Fazeela Yaqoob − *Department of Psychiatry, Perelman School of Medicine, University of Pennsylvania, Philadelphia, Pennsylvania 19104, United States*

Emily Han − *Department of Bioengineering, University of Pennsylvania, Philadelphia, Pennsylvania 19104, United States*

Kelsey L. Swingle − *Department of Bioengineering, University of Pennsylvania, Philadelphia, Pennsylvania 19104, United States;* orcid.org/0000-0001-8475-9206

Pallavi Menon − *Center for Fetal Research, Children's Hospital of Philadelphia, Philadelphia, Pennsylvania 19104, United States*

Emily Hodgson − *Center for Fetal Research, Children's Hospital of Philadelphia, Philadelphia, Pennsylvania 19104, United States*

Arijit Biswas − *Duke-NUS Graduate Medical School, Singapore 169547, Singapore*

Margaret M. Billingsley − *Department of Bioengineering, University of Pennsylvania, Philadelphia, Pennsylvania 19104, United States;* orcid.org/0000-0003-4499-9066

Li Li − *Cardiovascular Institute, Perelman School of Medicine, University of Pennsylvania, Philadelphia, Pennsylvania 19104, United States*

Fan Yiping − *Duke-NUS Graduate Medical School, Singapore 169547, Singapore*

Marco Carpenter − *Center for Fetal Research, Children's Hospital of Philadelphia, Philadelphia, Pennsylvania 19104, United States*

Alexandra Trokhan − *Center for Fetal Research, Children's Hospital of Philadelphia, Philadelphia, Pennsylvania 19104, United States*

Julie Yeo − *Duke-NUS Graduate Medical School, Singapore 169547, Singapore*

Nuryanti Johana − *Duke-NUS Graduate Medical School, Singapore 169547, Singapore*

https://doi.org/10.1021/acsnano.3c02268
ACS Nano XXXX, XXX, XXX−XXX

Tan Yi Wan − *Duke-NUS Graduate Medical School, Singapore 169547, Singapore*
Mohamad-Gabriel Alameh − *Department of Medicine, Perelman School of Medicine, University of Pennsylvania, Philadelphia, Pennsylvania 19104, United States;* orcid.org/0000-0002-5672-6930
Frederick Chris Bennett − *Department of Psychiatry, Perelman School of Medicine, University of Pennsylvania, Philadelphia, Pennsylvania 19104, United States*
Phillip B. Storm − *Division of Neurosurgery, Children's Hospital of Philadelphia, Philadelphia, Pennsylvania 19104, United States*
Rajan Jain − *Department of Medicine, Perelman School of Medicine, University of Pennsylvania, Philadelphia, Pennsylvania 19104, United States; Cardiovascular Institute, Perelman School of Medicine, University of Pennsylvania, Philadelphia, Pennsylvania 19104, United States*
Jerry Chan − *Duke-NUS Graduate Medical School, Singapore 169547, Singapore; Department of Reproductive Medicine, KK Women's and Children's Hospital, Singapore 229899, Singapore*
Drew Weissman − *Department of Medicine, Perelman School of Medicine, University of Pennsylvania, Philadelphia, Pennsylvania 19104, United States;* orcid.org/0000-0002-1501-6510

Complete contact information is available at: https://pubs.acs.org/10.1021/acsnano.3c02268

Author Contributions

●R.P. and S.K.B. made an equal contribution and contributed to experimental design, data collection, analysis, and interpretation. A.D. and B.M.W. contributed to all data collection and analysis. P.M. and A.T. contributed to cell culture and preparation of samples for sequencing analysis. E.Ha contributed to the preparation of LNPs used in this study. E.Ho. contributed to the design, execution, and analysis of ELISA studies conducted in this study. F.Ya. and F.C.B. contributed to the design, execution, and analysis of mouse histology generated in this study. K.L.S. and M.M.B. contributed to the characterization of LNPs. A.B., F.Yi., J.Y., N.J., T.Y.W., and J.C. executed the injection and harvest of the fetal NHP. C.B., V.L., M.C., L.L., and R.J. contributed to the design, execution, and analysis of macaque histology generated in this study. M.-G.A. and D.W. contributed to the design and synthesis of mRNA utilized in this study and critically reviewed the manuscript. P.B.S. provided patient brain tissue used in this study. R.P., W.H.P., and M.J.M. contributed to writing of this manuscript. W.H.P. and M.J.M equally contributed to the direction of the project and experimental design, data analysis, and interpretation.

Funding

This study was supported by the U.S. National Institutes of Health (NIH) Director's New Innovator Awards (DP2TR002776 to M.J.M and DP2HL152427 to W.H.P), NIH R01DK123049 to W.H.P. and M.J.M, and a Burroughs Wellcome Fund Career Award at the Scientific Interface (CASI) to M.J.M. R.P. was supported by an NIH Medical Scientist Training Program grant (T32GM07170) and an NIH NHLBI F30 fellowship (F30HL162465−01A1).

Notes

The authors declare the following competing financial interest(s): R.P., W.H.P., and M.J.M. have filed a patent application based on this work. D.W. is an inventor on several patents related to this work filed by the Trustees of the University of Pennsylvania (11/990,646; 13/585,517, 13/839,023; 13/839,155; 14/456,302; 15/339,363; and 16/299,202). M.J.M. is an inventor on a patent related to this work filed by the Trustees of the University of Pennsylvania (PCT/US20/56252). The authors declare that they have no other competing interests.

ACKNOWLEDGMENTS

We acknowledge the Children's Hospital of Philadelphia Small Animal Imaging Facility for maintenance of the IVIS. Figure schematics were created with BioRender.

REFERENCES

(1) Eisengart, J. B.; Pierpont, E. I.; Kaizer, A. M.; Rudser, K. D.; King, K. E.; Pasquali, M.; Polgreen, L. E.; Dickson, P. I.; Le, S. Q.; Miller, W. P.; Tolar, J.; Orchard, P. J.; Lund, T. C. Intrathecal enzyme replacement for Hurler syndrome: biomarker association with neurocognitive outcomes. *Genet. Med.* **2019**, *21*, 2552−2560.
(2) Freeze, H.; Eklund, E. A.; Ng, B.; Patterson, M. C. Neurology of inherited glycosylation disorders. *Lancet Neurol.* **2012**, *11*, 453−466.
(3) Peranteau, W. H.; Flake, A. W. The Future of In Utero Gene Therapy. *Mol. Diagn. Ther.* **2020**, *24*, 135−142.
(4) Palanki, R.; Peranteau, W. H.; Mitchell, M. J. Delivery Technologies for In Utero Gene Therapy. *Adv. Drug Delivery Rev.* **2021**, *169*, 51.
(5) Cox, D. B. T.; Platt, R. J.; Zhang, F. Therapeutic Genome Editing: Prospects and Challenges. *Nat. Med.* **2015**, *21*, 121−131.
(6) Anzalone, A. V.; Koblan, L. W.; Liu, D. R. Genome editing with CRISPR−Cas nucleases, base editors, transposases and prime editors. *Nat. Biotechnol.* **2020**, *38*, 824−844.
(7) Rossidis, A. C.; Stratigis, J. D.; Chadwick, A. C.; Hartman, H. A.; Ahn, N. J.; Li, H.; Singh, K.; Coons, B. E.; Li, L.; Lv, W.; Zoltick, P. W.; Alapati, D.; Zacharias, W.; Jain, R.; Morrisey, E. E.; Musunuru, K.; Peranteau, W. H. In utero CRISPR-mediated therapeutic editing of metabolic genes. *Nat. Med.* **2018**, *24*, 1513−1518.
(8) Alapati, D.; Zacharias, W. J.; Hartman, H. A.; Rossidis, A. C.; Stratigis, J. D.; Ahn, N. J.; Coons, B.; Zhou, S.; Li, H.; Singh, K.; Katzen, J.; Tomer, Y.; Chadwick, A. C.; Musunuru, K.; Beers, M. F.; Morrisey, E. E.; Peranteau, W. H. In utero gene editing for monogenic lung disease. *Sci. Transl. Med.* **2019**, *11*, No. eaav8375.
(9) Bose, S. K.; White, B. M.; Kashyap, M. V.; Dave, A.; De Bie, F. R.; Li, H.; Singh, K.; Menon, P.; Wang, T.; Teerdhala, S.; Swaminathan, V.; Hartman, H. A.; Jayachandran, S.; Chandrasekaran, P.; Musunuru, K.; Jain, R.; Frank, D. B.; Zoltick, P.; Peranteau, W. H. In utero adenine base editing corrects multi-organ pathology in a lethal lysosomal storage disease. *Nat. Commun.* **2021**, *12*, 4291.
(10) Paunovska, K.; Loughrey, D.; Dahlman, J. E. Drug delivery systems for RNA therapeutics. *Nat. Rev. Genet.* **2022**, *23*, 265−280.
(11) Bulcha, J. T.; Wang, Y.; Ma, H.; Tai, P. W. L.; Gao, G. Viral vector platforms within the gene therapy landscape. *Signal Transduct. Target. Ther.* **2021**, *6*, 53.
(12) x, y High-dose AAV gene therapy deaths. *Nat. Biotechnol.* **2020**, *38*, 910−910.
(13) Huang, X.; Kong, N.; Zhang, X.; Cao, Y.; Langer, R.; Tao, W. The landscape of mRNA nanomedicine. *Nat. Med.* **2022**, *28*, 2273−2287.
(14) Xiao, Y.; Tang, Z.; Huang, X.; Chen, W.; Zhou, J.; Liu, H.; Liu, C.; Kong, N.; Tao, W. Emerging mRNA technologies: delivery strategies and biomedical applications. *Chem. Soc. Rev.* **2022**, *51*, 3828−3845.
(15) Song, C.-Q.; Jiang, T.; Richter, M.; Rhym, L. H.; Koblan, L. W.; Zafra, M. P.; Schatoff, E. M.; Doman, J. L.; Cao, Y.; Dow, L. E.; Zhu, L. J.; Anderson, D. G.; Liu, D. R.; Yin, H.; Xue, W. Adenine base

editing in an adult mouse model of tyrosinaemia. *Nat. Biomed. Eng.* **2020**, *4*, 125−130.
(16) Musunuru, K.; Chadwick, A. C.; Mizoguchi, T.; Garcia, S. P.; DeNizio, J. E.; Reiss, C. W.; Wang, K.; Iyer, S.; Dutta, C.; Clendaniel, V.; Amaonye, M.; Beach, A.; Berth, K.; Biswas, S.; Braun, M. C.; Chen, H.-M.; Colace, T. V.; Ganey, J. D.; Gangopadhyay, S. A.; Garrity, R.; Kasiewicz, L. N.; Lavoie, J.; Madsen, J. A.; Matsumoto, Y.; Mazzola, A. M.; Nasrullah, Y. S.; Nneji, J.; Ren, H.; Sanjeev, A.; Shay, M.; Stahley, M. R.; Fan, S. H. Y.; Tam, Y. K.; Gaudelli, N. M.; Ciaramella, G.; Stolz, L. E.; Malyala, P.; Cheng, C. J.; Rajeev, K. G.; Rohde, E.; Bellinger, A. M.; Kathiresan, S. In vivo CRISPR base editing of PCSK9 durably lowers cholesterol in primates. *Nature* **2021**, *593*, 429−434.
(17) Gillmore, J. D.; Gane, E.; Taubel, J.; Kao, J.; Fontana, M.; Maitland, M. L.; Seitzer, J.; O'Connell, D.; Walsh, K. R.; Wood, K.; Phillips, J.; Xu, Y.; Amaral, A.; Boyd, A. P.; Cehelsky, J. E.; McKee, M. D.; Schiermeier, A.; Harari, O.; Murphy, A.; Kyratsous, C. A.; Zambrowicz, B.; Soltys, R.; Gutstein, D. E.; Leonard, J.; Sepp-Lorenzino, L.; Lebwohl, D. CRISPR-Cas9 In Vivo Gene Editing for Transthyretin Amyloidosis. *N. Engl. J. Med.* **2021**, *385*, 493−502.
(18) Han, X.; Zhang, H.; Butowska, K.; Swingle, K. L.; Alameh, M.-G.; Weissman, D.; Mitchell, M. J. An ionizable lipid toolbox for RNA delivery. *Nat. Commun.* **2021**, *12*, 7233.
(19) Riley, R. S.; Kashyap, M. V.; Billingsley, M. M.; White, B.; Alameh, M.-G.; Bose, S. K.; Zoltick, P. W.; Li, H.; Zhang, R.; Cheng, A. Y.; Weissman, D.; Peranteau, W. H.; Mitchell, M. J. Ionizable lipid nanoparticles for in utero mRNA delivery. *Sci. Adv.* **2021**, *7*, No. eaba1028.
(20) Kauffman, K. J.; Dorkin, J. R.; Yang, J. H.; Heartlein, M. W.; DeRosa, F.; Mir, F. F.; Fenton, O. S.; Anderson, D. G. Optimization of Lipid Nanoparticle Formulations for mRNA Delivery in Vivo with Fractional Factorial and Definitive Screening Designs. *Nano Lett.* **2015**, *15*, 7300−7306.
(21) Oberli, M. A.; Reichmuth, A. M.; Dorkin, J. R.; Mitchell, M. J.; Fenton, O. S.; Jaklenec, A.; Anderson, D. G.; Langer, R.; Blankschtein, D. Lipid Nanoparticle Assisted mRNA Delivery for Potent Cancer Immunotherapy. *Nano Lett.* **2017**, *17*, 1326−1335.
(22) Hajj, K. A.; Ball, R. L.; Deluty, S. B.; Singh, S. R.; Strelkova, D.; Knapp, C. M.; Whitehead, K. A. Branched-Tail Lipid Nanoparticles Potently Deliver mRNA In Vivo due to Enhanced Ionization at Endosomal pH. *Small* **2019**, *15*, 1805097.
(23) Basha, G.; Novobrantseva, T. I.; Rosin, N.; Tam, Y. Y. C.; Hafez, I. M.; Wong, M. K.; Sugo, T.; Ruda, V. M.; Qin, J.; Klebanov, B.; Ciufolini, M.; Akinc, A.; Tam, Y. K.; Hope, M. J.; Cullis, P. R. Influence of Cationic Lipid Composition on Gene Silencing Properties of Lipid Nanoparticle Formulations of siRNA in Antigen-Presenting Cells. *Mol. Ther.* **2011**, *19*, 2186−2200.
(24) Ratajczak, C. K.; Fay, J. C.; Muglia, L. J. Preventing preterm birth: the past limitations and new potential of animal models. *Dis. Model. Mech.* **2010**, *3*, 407−414.
(25) Cohen-Pfeffer, J. L.; Gururangan, S.; Lester, T.; Lim, D. A.; Shaywitz, A. J.; Westphal, M.; Slavc, I. Intracerebroventricular Delivery as a Safe, Long-Term Route of Drug Administration. *Pediatr. Neurol.* **2017**, *67*, 23−35.
(26) Pardi, N.; Tuyishime, S.; Muramatsu, H.; Kariko, K.; Mui, B. L.; Tam, Y. K.; Madden, T. D.; Hope, M. J.; Weissman, D. Expression kinetics of nucleoside-modified mRNA delivered in lipid nanoparticles to mice by various routes. *J. Controlled Release* **2015**, *217*, 345−351.
(27) Mattar, C. N.; Wong, A. M. S.; Hoefer, K.; Alonso-Ferrero, M. E.; Buckley, S. M. K.; Howe, S. J.; Cooper, J. D.; Waddington, S. N.; Chan, J. K. Y.; Rahim, A. A. Systemic gene delivery following intravenous administration of AAV9 to fetal and neonatal mice and late-gestation nonhuman primates. *FASEB J.* **2015**, *29*, 3876−3888.
(28) Swingle, K. L.; Billingsley, M. M.; Bose, S. K.; White, B.; Palanki, R.; Dave, A.; Patel, S. K.; Gong, N.; Hamilton, A. G.; Alameh, M.-G.; Weissman, D.; Peranteau, W. H.; Mitchell, M. J. Amniotic fluid stabilized lipid nanoparticles for in utero intra-amniotic mRNA delivery. *J. Control. Release Off. J. Control. Release Soc.* **2022**, *341*, 616−633.
(29) Hou, X.; Zaks, T.; Langer, R.; Dong, Y. Lipid nanoparticles for mRNA delivery. *Nat. Rev. Mater.* **2021**, *6*, 1078−1094.
(30) Billingsley, M. M.; Hamilton, A. G.; Mai, D.; Patel, S. K.; Swingle, K. L.; Sheppard, N. C.; June, C. H.; Mitchell, M. J. Orthogonal Design of Experiments for Optimization of Lipid Nanoparticles for mRNA Engineering of CAR T Cells. *Nano Lett.* **2022**, *22*, 533−542.
(31) Gary, D. J.; Min, J. B.; Kim, Y.; Park, K.; Won, Y.-Y. The Effect of N/P Ratio on the In Vitro and In Vivo Interaction Properties of PEGylated Poly(2-(dimethylamino)ethyl methacrylate)-Based siRNA Complexes. *Macromol. Biosci.* **2013**, *13*, 1059−1071.
(32) Wang, D.; Shukla, C.; Liu, X.; Schoeb, T. R.; Clarke, L. A.; Bedwell, D. M.; Keeling, K. M. Characterization of an MPS I-H knock-in mouse that carries a nonsense mutation analogous to the human IDUA-W402X mutation. *Mol. Genet. Metab.* **2010**, *99*, 62−71.
(33) Estapé Senti, M.; de Jongh, C. A.; Dijkxhoorn, K.; Verhoef, J. J. F.; Szebeni, J.; Storm, G.; Hack, C. E.; Schiffelers, R. M.; Fens, M. H.; Boross, P. Anti-PEG antibodies compromise the integrity of PEGylated lipid-based nanoparticles via complement. *J. Controlled Release* **2022**, *341*, 475−486.
(34) Szebeni, J.; Storm, G.; Ljubimova, J. Y.; Castells, M.; Phillips, E. J.; Turjeman, K.; Barenholz, Y.; Crommelin, D. J. A.; Dobrovolskaia, M. A. Applying lessons learned from nanomedicines to understand rare hypersensitivity reactions to mRNA-based SARS-CoV-2 vaccines. *Nat. Nanotechnol.* **2022**, *17*, 337−346.
(35) Riley, J. S.; McClain, L. E.; Stratigis, J. D.; Coons, B. E.; Ahn, N. J.; Li, H.; Loukogeorgakis, S. P.; Fachin, C. G.; Dias, A. I. B. S.; Flake, A. W.; Peranteau, W. H. Regulatory T cells promote alloengraftment in a model of late-gestation in utero hematopoietic cell transplantation. *Blood Adv.* **2020**, *4*, 1102−1114.
(36) Schwarz, N.; Uysal, B.; Welzer, M.; Bahr, J. C.; Layer, N.; Löffler, H.; Stanaitis, K.; PA, H.; Weber, Y. G.; Hedrich, U. B.; Honegger, J. B.; Skodras, A.; Becker, A. J.; Wuttke, T. V.; Koch, H.; Slutsky, I.; Marder, E.; Mansvelder, H. D. Eds. Long-term adult human brain slice cultures as a model system to study human CNS circuitry and disease. *eLife* **2019**, *8*, No. e48417.
(37) Ingusci, S.; Verlengia, G.; Soukupova, M.; Zucchini, S.; Simonato, M. Gene Therapy Tools for Brain Diseases. *Front. Pharmacol.* **2019**, *10*, 00724.
(38) Clarke, L. A *Mucopolysaccharidosis Type I*; University of Washington, Seattle: 2021.
(39) Akaishi, T.; Onishi, E.; Abe, M.; Toyama, H.; Ishizawa, K.; Kumagai, M.; Kubo, R.; Nakashima, I.; Aoki, M.; Yamauchi, M.; Ishii, T. The human central nervous system discharges carbon dioxide and lactic acid into the cerebrospinal fluid. *Fluids Barriers CNS* **2019**, *16*, 8.
(40) Villiger, L.; Rothgangl, T.; Witzigmann, D.; Oka, R.; Lin, P. J. C.; Qi, W.; Janjuha, S.; Berk, C.; Ringnalda, F.; Beattie, M. B.; Stoffel, M.; Thöny, B.; Hall, J.; Rehrauer, H.; van Boxtel, R.; Tam, Y. K.; Schwank, G. In vivo cytidine base editing of hepatocytes without detectable off-target mutations in RNA and DNA. *Nat. Biomed. Eng.* **2021**, *5*, 179−189.
(41) Massaro, G.; Mattar, C. N. Z.; Wong, A. M. S.; Sirka, E.; Buckley, S. M. K.; Herbert, B. R.; Karlsson, S.; Perocheau, D. P.; Burke, D.; Heales, S.; Richard-Londt, A.; Brandner, S.; Huebecker, M.; Priestman, D. A.; Platt, F. M.; Mills, K.; Biswas, A.; Cooper, J. D.; Chan, J. K. Y.; Cheng, S. H.; Waddington, S. N.; Rahim, A. A. Fetal gene therapy for neurodegenerative disease of infants. *Nat. Med.* **2018**, *24*, 1317−1323.
(42) Benatti, H. R.; Gray-Edwards, H. L. Adeno-Associated Virus Delivery Limitations for Neurological Indications. *Hum. Gene Ther.* **2022**, *33*, 1−7.
(43) Dilliard, S. A.; Cheng, Q.; Siegwart, D. J. On the mechanism of tissue-specific mRNA delivery by selective organ targeting nanoparticles. *Proc. Natl. Acad. Sci. U. S. A.* **2021**, *118*, No. e2109256118.
(44) Dayon, L.; Cominetti, O.; Wojcik, J.; Galindo, A. N.; Oikonomidi, A.; Henry, H.; Migliavacca, E.; Kussmann, M.; Bowman, G. L.; Popp, J. Proteomes of Paired Human Cerebrospinal

https://doi.org/10.1021/acsnano.3c02268
ACS Nano XXXX, XXX, XXX−XXX

Fluid and Plasma: Relation to Blood−Brain Barrier Permeability in Older Adults. *J. Proteome Res.* **2019**, *18*, 1162−1174.
(45) Kim, J.-Y.; Grunke, S. D.; Levites, Y.; Golde, T. E.; Jankowsky, J. L. Intracerebroventricular Viral Injection of the Neonatal Mouse Brain for Persistent and Widespread Neuronal Transduction. *JoVE J. Vis. Exp.* **2014**, No. e51863.
(46) Cetin, A.; Komai, S.; Eliava, M.; Seeburg, P. H.; Osten, P. Stereotaxic gene delivery in the rodent brain. *Nat. Protoc.* **2006**, *1*, 3166−3173.
(47) Park, T. I.-H.; Schweder, P.; Lee, K.; Dieriks, B. V.; Jung, Y.; Smyth, L.; Rustenhoven, J.; Mee, E.; Heppner, P.; Turner, C.; Curtis, M. A.; Faull, R. L. M.; Montgomery, J. M.; Dragunow, M. Isolation and culture of functional adult human neurons from neurosurgical brain specimens. *Brain Commun.* **2020**, *2*, fcaa171.

https://doi.org/10.1021/acsnano.3c02268
ACS Nano XXXX, XXX, XXX−XXX